Renewable and Sustainable Energy Reviews 58 (2016) 1189–1206

Contents lists available at ScienceDirect

Renewable and Sustainable Energy Reviews

journal homepage: www.elsevier.com/locate/rser

Review on supercapacitors: Technologies and materials

Ander González [a,b], Eider Goikolea [b], Jon Andoni Barrena [a], Roman Mysyk [b,*]

[a] Mondragon Unibertsitatea, Loramendi 4, 20500 Arrasate, Spain
[b] CIC Energigune, Albert Einstein 48, 01510 Miñano, Spain

ARTICLE INFO

Article history:
Received 17 July 2014
Received in revised form
7 September 2015
Accepted 27 December 2015
Available online 15 January 2016

Keywords:
Supercapacitor
Electric double-layer
Pseudocapacitance
Electrode material
Electrolyte

ABSTRACT

In this review, the technologies and working principles of different materials used in supercapacitors are explained. The most important supercapacitor active materials are discussed from both research and application perspectives, together with brief explanations of their properties, such as specific surface area and capacitance values. A review of different supercapacitor electrolytes is given and their positive and negative features are discussed. Finally, cell configurations are considered, pointing out the advantages and drawbacks of each configuration.

Contents

1. Introduction . . . 1190
2. Supercapacitors within energy storage systems . . . 1190
3. Electric double layer . . . 1193
   3.1. Helmholtz model . . . 1193
   3.2. Gouy–Chapman or diffuse model . . . 1194
   3.3. Stern modification of the diffuse double layer . . . 1194
   3.4. Electric double layer in supercapacitors . . . 1194
4. Pseudocapacitance . . . 1194
5. Electrode materials . . . 1195
   5.1. Carbon materials . . . 1195
      5.1.1. Activated carbon . . . 1195
      5.1.2. Carbide derived carbons (CDC) . . . 1196
      5.1.3. Carbon nanotubes (CNT) . . . 1196
      5.1.4. Graphene . . . 1197
      5.1.5. Mesoporous carbons . . . 1198
   5.2. Metal oxides . . . 1198
      5.2.1. Ruthenium oxide . . . 1198
      5.2.2. Manganese oxide . . . 1199
   5.3. Polymers . . . 1199
6. Electrolytes . . . 1200
   6.1. Aqueous and organic electrolytes . . . 1200
   6.2. Ionic liquids . . . 1200
7. Electrochemical configuration of supercapacitor cells . . . 1201
   7.1. Lithium-ion capacitors . . . 1201

* Corresponding author. Tel.: +34 94 529 71 08; fax: +34 94 529 71 08.
E-mail address: rmysyk@cicenergigune.com (R. Mysyk).

http://dx.doi.org/10.1016/j.rser.2015.12.249
1364-0321/

8. Manufacturers . . . 1202
9. Conclusions . . . 1202
References . . . 1202

1. Introduction

The increasing cost of fuels, pollution, global warming and geopolitical concerns are among the problems connected with the dependence of modern societies on fossil fuels. Reducing these issues is an increasingly important goal that can be achieved through developing other energy sources and storage technologies. As a result, recently there has been a growing interest in high power and high energy density storage systems. A more widespread use of renewable sources and a better efficiency of transportation systems are two important goals to be pursued to overcome this problem.

Energy storage systems (ESSs) are the key to deal with the intermittent nature of renewable energy sources and increase the power transmitted into the grid from systems such as wind and solar power. In addition, an increase in the efficiency of a vehicle requires kinetic energy to be stored somewhere whenever the vehicle slows down or stops. Although these operations have been successfully performed with batteries on a low-power scale, new methods for efficiency enhancement will require large amounts of power that can only be provided by other energy storage technologies such as supercapacitors. These have attracted significant attention due to their high power capabilities and long cycle-life, giving a very good chance to build more advanced hybrid ESSs, for both on-board and stationary applications.

2. Supercapacitors within energy storage systems

Supercapacitors are devices capable of managing high power rates compared to batteries. Although supercapacitors provide hundred to many thousand times higher power in the same volume [1], they are not able to store the same amount of charge as batteries do, which is usually 3–30 times lower [1]. This makes supercapacitors suitable for those applications in which power bursts are needed, but high energy storage capacity is not required. Supercapacitors can also be included within a battery-based ESS to decouple the power and energy characteristics of the ESS, thus improving the sizing while fulfilling the power and energy requirements, and probably enlarging its lifetime.

The power output of supercapacitors is lower than that of electrolytic capacitors, but can reach about 10 kW kg^{-1}. On the other hand, their specific energy is several orders of magnitude higher than the one of capacitors [2]. These devices are interesting because they fill the gap between aluminum electrolytic capacitors and batteries, which are capable of storing large amounts of energy, but do not offer very high power densities (< 1 kW kg^{-1}) due to their storage mechanism. This can be graphically explained in a Ragone plot, in which the energy and power densities are represented in horizontal and vertical axes, also showing the discharge time of the devices in diagonal lines ($E=Pt$). Different storage technologies are represented in a Ragone plot in Fig. 1. However, the Ragone plot does not reflect many other performance parameters such as cost, safety and cycle life. They need to be mentioned separately for a complete understanding of advantages and limitations of a particular energy storage technology.

Thus, it is extremely important to note that supercapacitors can not only be discharged in a matter of seconds, but also be charged in such a short time period. This is an important benefit for energy recovery systems, e.g. for dynamic braking of transport systems. Table 1 compares supercapacitors with capacitors and batteries.

Another great advantage of supercapacitors is their cycle life. These devices can withstand millions of cycles thanks to their charge storage mechanism, which does not involve irreversible chemical reactions, storing charges physically at the surface of the electrodes in an electric double layer. This allows exceeding the cycle life of batteries, which are at best capable of withstanding a few thousand cycles. The highly reversible electrostatic storage does not produce changes in the electrode volume, eliminating the swelling occurring in typical redox reactions in the bulk of a

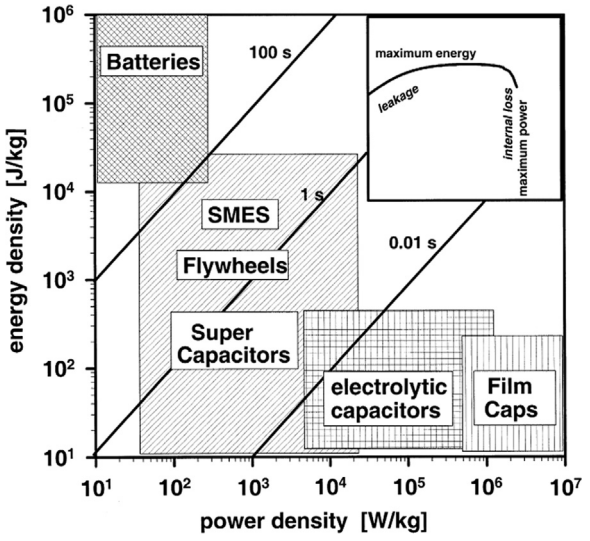

Fig. 1. Ragone plot. Detail window shows energy drop due to internal dissipation and leakage losses for sufficiently high and low power [185].

Table 1
Comparison table among selected electrochemical energy storage technologies.

Characteristics	Capacitor	Supercapacitor	Battery
Specific energy (W h kg^{-1})	< 0.1	1–10	10–100
Specific power (W kg^{-1})	$\geqslant 10,000$	500–10,000	< 1000
Discharge time	10^{-6} to 10^{-3}	s to min	0.3–3 h
Charge time	10^{-6} to 10^{-3}	s to min	1–5 h
Coulombic efficiency (%)	About 100	85–98	70–85
Cycle-life	Almost infinite	$> 500,000$	about 1000

* Data taken from [2].

Table 2
Comparison between batteries and supercapacitors [1].

Comparison parameter	Battery	Supercapacitor
Storage mechanism	Chemical	Physical
Power limitation	Reaction kinetics, mass transport	Electrolyte conductivity
Energy storage	High (bulk)	Limited (surface area)
Charge rate	Kinetically limited	High, same as discharge
Cycle life limitations	Mechanical stability, chemical reversibility	Side reactions

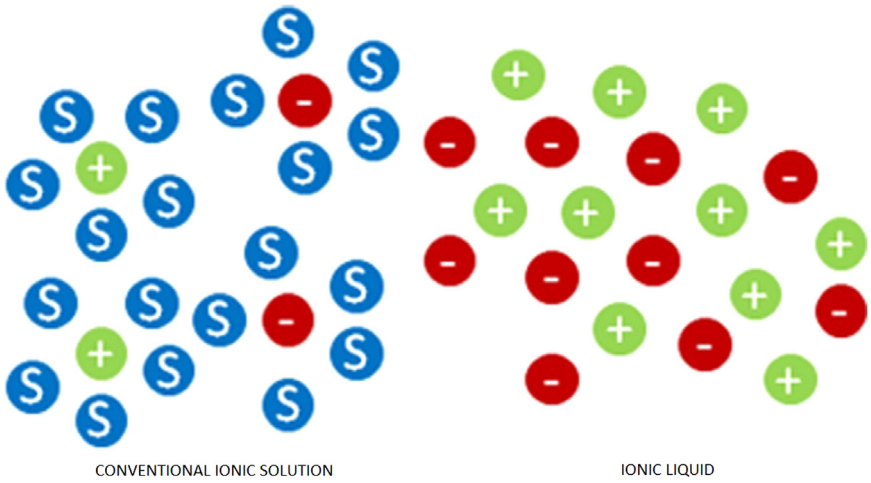

Fig. 2. Schematic difference between ionic liquids and conventional electrolytes based on dissolved salts [186]. "+" and "−" denote the cations and the anions, correspondingly, S – the solvent.

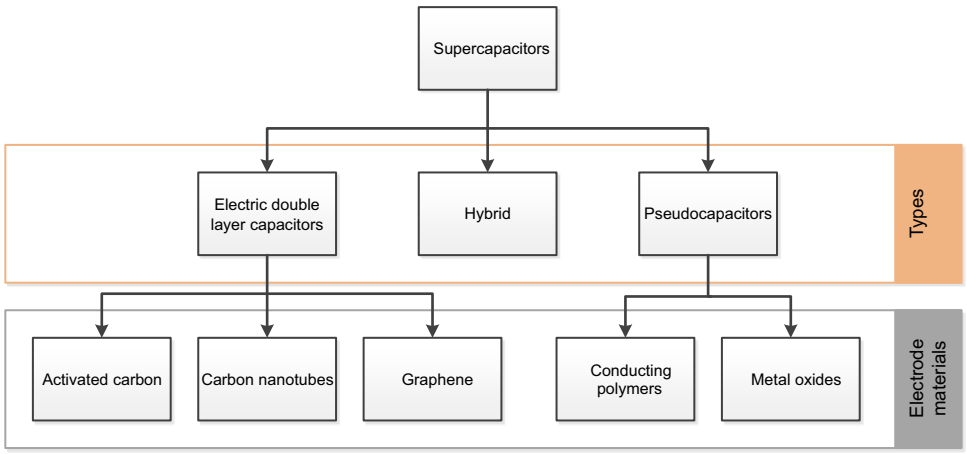

Fig. 3. Classification of different supercapacitors.

battery's active material during charge and discharge cycles. A supercapacitor electrode has no such rate limitations as those of redox battery electrodes due to electrochemical kinetics through a polarization resistance [3]. The main disadvantage related to the charge storage mechanism is the operating voltage of a supercapacitor cell, which should be kept low in order to avoid the chemical decomposition of electrolytes. Table 2 compares the main differences in the properties of batteries and supercapacitors.

The working temperature range is another feature to be pointed out. High power performance down to −40 °C can be achieved with supercapacitors [3], which is not possible at the moment with batteries. Besides, supercapacitors are generally safer than batteries for high power-rating charging and discharging [1]. Double layer capacitor cells do not rely on metals chemistries and do not thus run the risk of metal plating, which is an important battery degradation and failure mechanism as well as a safety concern that can lead to short circuits and uncontrollably energetic chemical reactions.

A supercapacitor cell comprises two electrodes with a separator between them. The electrodes can be identical for symmetric cells or different for asymmetric cells. The separator is soaked in electrolyte and prevents the electrical contact between the electrodes. The separator material should be ion-permeable, to allow the ionic charge transfer, while at the same time having a high electrical resistance, high ionic conductance, and low thickness in order to achieve the best performance. Usually polymer or paper separators are used together with organic electrolytes while ceramic or glass fiber separators are usually coupled with aqueous electrolytes [4]. The electrolyte breakdown potential at one of the electrodes limits the attainable cell voltage whereas the equivalent series resistance (ESR) of the cell will depend strongly on the electrolyte conductivity. Aqueous electrolytes typically have a breakdown voltage of around 1 V, which is significantly lower than the one achievable with organic electrolytes (around 3 V), but the conductivity of aqueous electrolytes is higher than that of organic electrolytes, which is desirable for high power devices. Aqueous electrolytes also feature such important assets as low cost and easiness in handling.

Depending on the storage mechanism or cell configuration, electric double-layer capacitors (EDLCs), pseudocapacitors, and hybrid capacitors can be distinguished. EDLCs are based on high specific-surface area ($>1000\ m^2g^{-1}$) nanoporous materials as active electrode materials, leading to a huge capacitance in comparison with electrostatic capacitors. The electrodes are usually made of nanoporous carbon materials thanks to their availability, existing industrial production and comparatively low cost. Pseudocapacitors are based on conducting polymer or metal oxide based electrodes, and sometimes functionalized porous carbons, combining electrostatic and pseudocapacitive charge storage mechanisms. These materials can hold much higher specific capacitance values as compared to EDLCs, with the charge storage mechanism relying on fast redox reactions occurring on the electrode surface but not in the bulk like in batteries. However, like in the case of batteries, redox reactions can lead to mechanical changes making the electrodes swell and shrink, giving rise to

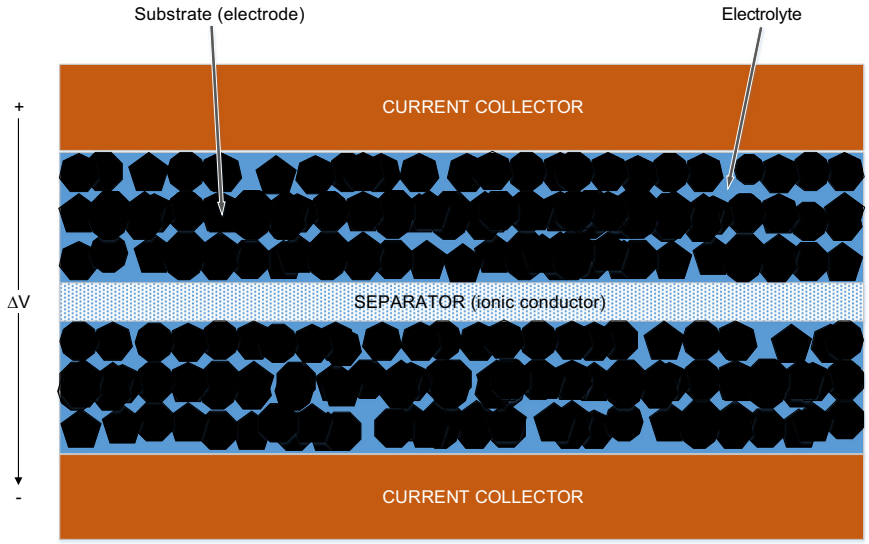

Fig. 4. Symmetric supercapacitor schematic diagram.

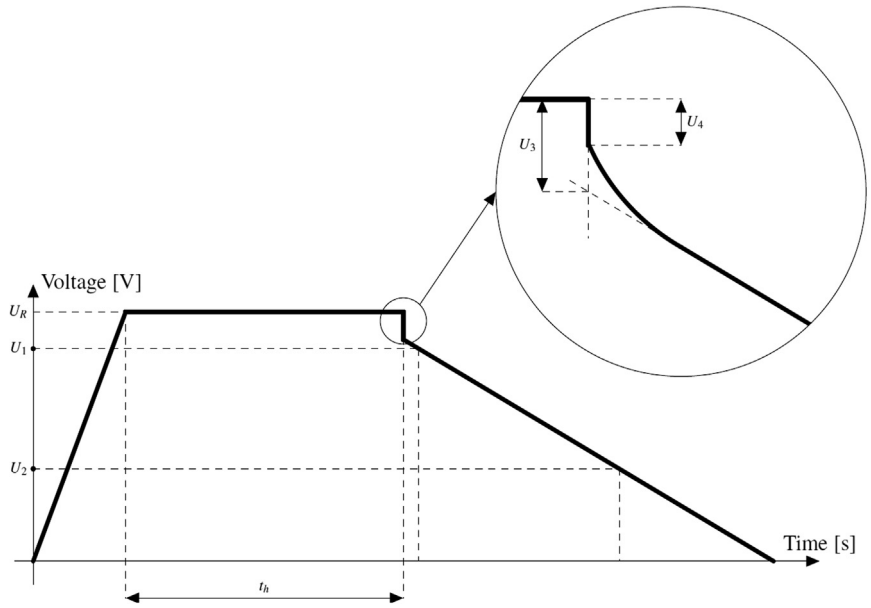

Fig. 5. Constant current discharge supercapacitor cell test.

poor mechanical stability. Consequently, lower cycle life is an important deficiency of pseudocapacitive materials. Finally, hybrid capacitors are composed of an EDLC electrode and a pseudocapacitive or battery type electrode, combining the properties of both systems and leading to an intermediate performance in some cases. A good example of such a system are the lithium-ion capacitors (LiCs). Different types of supercapacitors are classified in Fig. 3. Here two main research lines can be distinguished concerning pseudocapacitors and EDLCs [2].

As macroscopically these devices work like capacitors, the capacitance, C, will depend on the dielectric constant of the electrolyte, ε_r, the effective thickness of the double layer, d (separation between charges), and the accessible surface, A, as follows:

$$C = \frac{\varepsilon_r \varepsilon_0 A}{d} \tag{1}$$

where ε_0 is the dielectric constant of the vacuum. The capacitance for an electric double layer (EDL) on carbon surface varies usually from 5 to 20 μF cm^{-2} depending on the electrolyte [5], although much higher values are sometimes reported for edge carbon atoms.

The energy (E) stored within a supercapacitor is

$$E = \tfrac{1}{2} C V^2 \tag{2}$$

where V is the cell voltage. Formula (2) shows that the stored energy is proportional to both the capacitance of the device and the square of the cell voltage. Therefore, increasing both of them is a general strategy to increasing the energy density of the cell.

The maximum instantaneous power P_{max} that a supercapacitor is able to deliver, depends on the voltage and the internal resistance R as follows:

$$P_{max} = \frac{V^2}{4R} \tag{3}$$

Also the current across the supercapacitor will be

$$I = C\frac{dV}{dt} \tag{4}$$

In industry, constant current tests are performed to determine the main characteristics of devices. This includes capacitance calculation (integral of the area contained during the discharge), and resistances associated to the cell such as ESR and equivalent distributed resistance (EDR), which represents ESR and the resistance in the pores (part of the discharge with curvature). These are calculated using the notation in Fig. 5 with the following expressions:

$$C = \frac{I_{discharge} t_{discharge}}{U_1 - U_2} \quad (5)$$

$$ESR = \frac{U_4}{I_{discharge}} \quad (6)$$

$$EDR = \frac{U_3}{I_{discharge}} \quad (7)$$

The electrical properties of a supercapacitor are mainly determined by components such as electrode materials, electrolytes, separators and current collectors. Electrode fabrication is made through coating a metallic current collector with an about 100 μm thin layer of high surface area material. This active material is mixed with a binder so as to form slurry. The thickness of the slurry should be controlled for making the coated layer of active material sufficiently thin to be conductive throughout the material.

Since the ESR of supercapacitor cells must be very low, special attention must be paid to the contact resistance between the active material and the current collector. The surface of current collectors should be treated before coating it with active materials. Surface treatments decrease the Ohmic drop at the current collector/active material interface [6]. For supercapacitors designed to work with organic electrolytes, treated aluminum foils or grid current collectors are used. Using nanostructured current collectors with increased contact area is a way to control the current collector/active material interface [7].

A widely used measurement is the specific capacitance, which is the intrinsic capacitance of an electrode material expressed in F g^{-1}. Although this is a very useful characteristic of the material, a higher specific capacitance does not necessarily mean that the material will be a highly performing supercapacitor electrode. There are other factors substantially impacting capacitance such as electrical conductivity (both that of materials and between electrode particles), which governs electron and ion transfer into the layer [8].

3. Electric double layer

An electric double layer is a structure appearing when a charged object is placed into a liquid. The balancing counter charge for this charged surface will form on the liquid, concentrating near the surface. There are several theories or models for this interface between a solid and a liquid. In Fig. 6 the Helmholtz model, the Gouy–Chapman model and the Stern model are illustrated, where Ψ is the potential, Ψ_0 is the electrode potential, IHP refers to the inner Helmholtz plane, and OHP refers to the outer Helmholtz plane explained in the Stern model.

In Fig. 6 the models explained below are illustrated, where ψ is the potential, ψ_0 the electrode potential, IHP refers to the inner Helmholtz plane, and OHP refers to the outer Helmholtz plane explained in the Stern model.

3.1. Helmholtz model

This theory is the simplest approximation for modeling the spatial charge distribution at double layer interfaces. The charge of the solid electronic conductor is neutralized by opposite sign ions at a *d* distance from the solid. This is the distance from the surface to the center of the ions. This theory considers rigid layers counterbalancing the charges from the solid. As of today, this is taken as

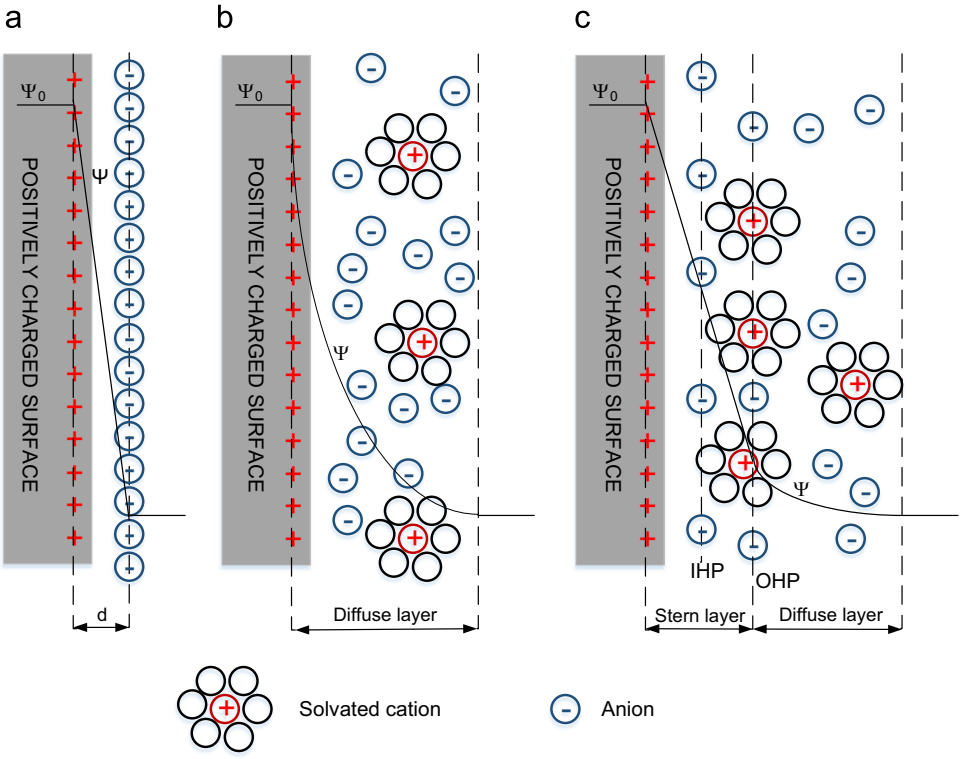

Fig. 6. EDL models, (a) Helmholtz model, (b) Gouy–Chapman model, and (c) Stern model.

the simplest theory, which does not adequately explain what occurs in nature [9,10].

3.2. Gouy–Chapman or diffuse model

Gouy suggests that the same amount of opposite ionic charge appears in a liquid surrounding a charged solid, but the ions are not rigidly attached to the surface [9]. These ions in the solution tend to diffuse into the liquid phase until the counter potential set up by their departure restricts this tendency. The kinetic energy of the ions in the solution will partially determine the thickness of the diffuse layer.

Gouy and Chapman developed theories of this diffuse layer in which the ion concentration in the solution near the surface follows the Boltzmann distribution. This model fails for highly charged double layers [10]. Experimentally, the measured thickness of double layers is greater than the calculated.

3.3. Stern modification of the diffuse double layer

The Gouy–Chapman model makes a better approach to the reality than the Helmholtz model, but still has limited quantitative applications. It assumes that the ions are point charges and that they can approach the surface with no limits, which is not true. Stern modified the Gouy–Chapman model stating that the ions have a finite size, so limiting their approach to the surface. The first ions in the Gouy–Chapman model are at the δ distance away from the surface, but the Stern model assumes that there can be specifically surface-adsorbed ions in plane δ, this is known as the Stern layer. Ions are strongly adsorbed by the electrode within this so-called compact layer. In the compact layer there are specifically adsorbed ions (forming the inner Helmholtz plane), and non-specifically adsorbed counter-ions (forming the outer Helmholtz plane) [11].

Summarizing, in order to resolve the shortcomings of the Gouy–Chapman model for the diffuse layer, Stern suggested the combination of both previous models, giving an internal Stern layer (e.g. the Helmholtz layer) and an outer diffuse layer (e.g. the Gouy–Chapman layer).

3.4. Electric double layer in supercapacitors

Although the above models give a satisfactory description of the electrical double layer on plane surfaces, they fall short of describing the real charge distribution in nanoporous electrodes employed in supercapacitors. The peculiarities of ion electrosorption in porous media make the process of charge storage extremely difficult, and there is still a lack of complete understanding of ions behavior in nanopores.

When a supercapacitor is charged, electrons are forced to go from the positive electrode to the negative electrode through an external circuit. As a consequence, cations within the electrolyte concentrate in the negative electrode and anions in the positive electrode forming an EDL that compensates the external charge unbalance. During the discharge, electrons travel from the negative electrode to the positive electrode through an external circuit, and both kinds of ions in the pores become mixed again until the cell is discharged.

Ions do not move in the bulk electrolyte the same way as they do within the pores of an electrode material. The mobility of ions into the pores is greatly influenced by the pore size, which if too small makes the pores inaccessible, not contributing to double layer capacitance [4].

Since not all the pores are accessible to the ions, there is no linear relation between the capacitance exhibited by a material and its specific surface area [12–15] measured with a small gas molecule probe such as N_2 or Ar. Various studies suggest that pore size below 0.5 nm is not accessible to hydrated ions [15,16], and pores smaller than 1 nm can be too small for organic electrolytes [17]. Generally, there is a controversy regarding the effect of pore size on capacitance. Chmiola et al. claimed that pores with sizes below 1 nm greatly contribute to the capacitance [18]. This increase was explained with the distortion of the solvation shell, thus reducing the distance between charges and enhancing the capacitance [5,19]. On the other hand, constant capacitance in the micropores was measured in organic electrolyte on the basis of a detailed assessment of pore size using complementary adsorption techniques. The decrease in the distance between the electronic and ionic charges is counterbalanced by the corresponding decrease in the effective dielectric permittivity inside the pores, which occurs due to gradual ion desolvation [20–22]. Leaving the controversy of capacitance vs. pore size behind, it is worth mentioning that industrially important values are also calculated on a volumetric basis. It then becomes clear that too wide pores contain free space, which is not used for capacitive charge storage, but decreases the density of electrodes. This effect is detrimental to volume-based capacitance as well as the existence of narrow electrolyte-inaccessible pores. Thus, tuning pore size is anyway needed to have carbon materials with narrow, short and electrolyte-accessible pores [18].

Apart from it, there is a general agreement that the power capability of a supercapacitor can be enhanced by the presence of a small amount of mesopores (pores wider than 2 nm) for a rapid supply of electrolyte to the micropore surface where main charge storage takes place [23].

There have been numerous attempts to properly describe the capacitance of carbon materials depending on the pore shape and size and the specific character of their interaction with electrolytes. For mesoporous carbons with cylindrical pores, the traditional model is used [24]:

$$\frac{C}{A}=\frac{\varepsilon_r\varepsilon_0}{b\ln\left(\frac{b}{b-d}\right)} \tag{8}$$

where b is the pore radius and d the distance between the ion and the carbon surface. But for micropores, it is assumed that the ions line up in the center of a cylindrical pore, so the capacitance is calculated from [24]:

$$\frac{C}{A}=\frac{\varepsilon_r\varepsilon_0}{b\ln\left(\frac{b}{a_0}\right)} \tag{9}$$

where a_0 is the effective size of the ion. This ionic radius was found to be close to the bare ion size, which means that the ions could be fully desolvated.

However, as the more realistic approximation to the pore shape in carbons is a slit, not a cylinder, a sandwich capacitance model was later proposed [25].

$$\frac{C_{tot}}{2A}=\frac{C_s}{A}=\frac{\varepsilon_r\varepsilon_0}{b-a_0} \tag{10}$$

4. Pseudocapacitance

Pseudocapacitance is a Faradaic charge storage mechanism based on fast and highly reversible surface or near-surface redox reactions. Importantly, the electrical response of a pseudocapacitive material is ideally the same as the one of a double-layer capacitor, i.e. the state of charge changes continuously with the potential, leading to proportionality constant that can be formally considered as capacitance. Some materials can also store a significant charge in a double layer such as functionalized porous

carbons, combining thus both capacitive and pseudocapacitive storage mechanisms.

A material's pseudocapacitance can be intrinsic or extrinsic [26]. In the first case, materials exhibit pseudocapacitive behavior in a broad range of particle size and morphologies. Extrinsic pseudocapacitance only appears under several conditions for nanosized material whereas the same material does not show pseudocapacitive behavior in the bulk. Kinetically, pseudocapacitive materials can be distinguished from battery-type materials through electroanalytical experiments, with their kinetics being limited by a surface-related process as opposed to diffusion-controlled reactions governing the electrochemical response of battery electrodes.

Different charge storage mechanisms can be distinguished in a pseudocapacitive electrode: underpotential deposition, redox reactions of transition metal oxides, intercalation pseudocapacitance [27], and also reversible electrochemical doping and de-doping in conducting polymers. Materials used for building such electrodes are normally carbons, metal oxides, and conducting polymers [1,28,8].

Faradic processes occurring together with EDL charge storage increase the specific capacitance of an electrode. The capacitance of a pseudocapacitor can be 10–100 times higher than that of an EDLC. Nevertheless, the power performance of a pseudocapacitor is usually lower than that of EDLCs, due to the slower Faradic processes involved [29].

Electrodes exhibiting pseudocapacitance are more prone to swelling and shrinking on charge/discharge cycling, which can lead to poor mechanical stability and low cycle life [30].

5. Electrode materials

The most important electrode materials are gathered here, giving a brief explanation of their characteristics. This section is divided in three subsections comprising carbon based materials, metal oxides, and conducting polymers.

5.1. Carbon materials

Carbon based materials are widely used in many applications. As they feature relatively low cost and an established industrial production processes, their availability is quite high. This section details carbons for supercapacitors, from the most widespread types to the newest developments. These materials show a nearly rectangular shape cyclic voltammogram as illustrated in Fig. 7 which presents cyclic voltammograms for carbon materials in both, aqueous and organic electrolytes.

5.1.1. Activated carbon

Activated carbon is the most widely used active material for supercapacitor electrodes due to its high surface area and relatively low cost [5,31,11]. These are obtained from carbon-rich organic precursors through a heat treatment under inert atmosphere (carbonization) and activation resulting in porosity formation. These precursors can be obtained from natural renewable resources such as coconut shells wood, fossil fuels and their derivatives such as pitch, coal or coke, or from synthetic precursors such as polymers [5,31].

Carbonization is the process of producing amorphous carbon by the thermal chemical conversion of precursors while activation leads to a high surface area. This is achieved through making a partial controlled oxidation of the carbon precursor grains by a physical or chemical activation [11]. Physical activation is done at high temperature under oxidizing atmosphere (e.g. CO_2, H_2O…) [31], whereas chemical activation is performed on amorphous carbons previously mixed with chemicals such as alkalis, carbonates, chlorides or acids (e.g. KOH [31], K_2CO_3…). The result of any activation process is the formation of a porous network in the bulk

Table 3
BET specific surface areas for different carbon precursors. Data taken from [37].

Carbon precursor	Activation method	S_{bet} ($m^2\ g^{-1}$)
Furfurol	Steam	1040
Coconut shell	KOH	1660
Eucalyptus wood	KOH	2970
Firwood	Steam	1130
Bamboo	KOH	1290
Cellulose	KOH	2460
Potato starch	KOH	2340
Starch	KOH	1510
Sucrose	CO_2	2100
Beer lees	KOH	3560
Banana fiber	$ZnCl_2$	1100
Corn grain	KOH	3200
Sugar cane bagasse	$ZnCl_2$	1790
Apricot shell	NaOH	2335
Sunflower seed shell	KOH	2510
Coffee ground	$ZnCl_2$	1020
Wheat straw	KOH	2316
Fish scale	–	2270
Cherry stone	KOH	1300
Rice husk	NaOH	1890
Rice husk	KOH	1390

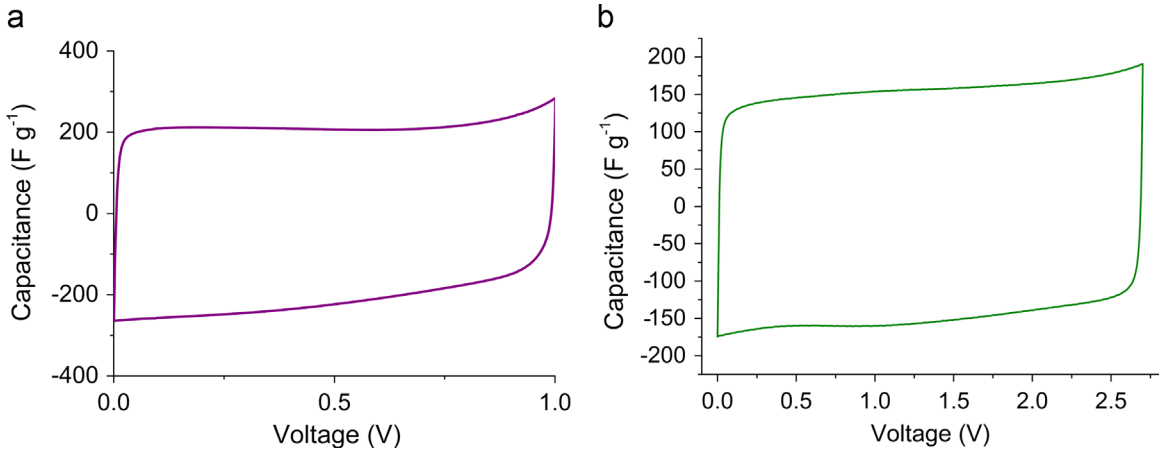

Fig. 7. Cyclic voltammogram of an EDLC cell at 5 mV s^{-1} in (a) aqueous 6 M KOH and (b) organic 1 M tetraethylammonium tetrafluoroborate electrolytes.

of the carbon particles with high specific surface area (SSA). Nanopores can be broken down according to their size, namely into micropores (<2 nm), mesopores (2–50 nm), and macropores (>50 nm). The accurate measurement of SSA is not a straightforward task, depending greatly on the calculation method and measurement conditions. Specific surface areas of 3000 $m^2\ g^{-1}$ are sometimes reported, but the useable SSA falls usually in the range of 1000–2000 $m^2\ g^{-1}$ [5]. Table 3 summarizes different precursors and the corresponding Brunauer–Emmett–Teller (BET) surface area values for activated carbons derived from them.

Most of the commercially available devices are constructed with activated carbon electrodes and organic electrolytes. These devices reach operating cell voltages of 2.7 V with a specific capacitance of 100–120 $F\ g^{-1}$ [32,33] and up to 60 $F\ cm^{-3}$ [5]. This can be illustrated by a few examples. As a promising material for mass production, low-cost carbon-rich biochar (red cedar) material was reported to achieve a gravimetric capacitance of 115 $F\ g^{-1}$ in aqueous electrolyte [34]. In [35] carbon hollow fibers were reported to achieve 287 $F\ g^{-1}$ at 50 $mA\ g^{-1}$ with a capacitance retention of 86.4% at 1 $A\ g^{-1}$. In [36] a specific capacitance of 340 $F\ g^{-1}$ was reported for carbon prepared by phosphoric acid activation from a sugarcane bagasse precursor. In aqueous electrolytes the operating cell voltage is limited to 0.9 V [5] and the specific capacitance reaches 300 $F\ g^{-1}$ [31].

Activated carbon powders can be mixed with carbon blacks and organic binders to make active material films, these films can be used to coat current collectors. The pore size distribution in activated carbon powders is in most cases broad and is often not optimized due to the difficulty of the activation process [5]. Longer activation times of activation or higher temperatures lead to a larger average pore size [31]. As explained above, the whole SSA of the material is underused, i.e. part of it does not contribute to capacitance [5].

5.1.2. Carbide derived carbons (CDC)

Carbide derived carbons (CDCs) are prepared by high-temperature extraction of metals from carbides serving as precursors. The most common methods for CDC production are high-temperature chlorination [38,39] and vacuum decomposition [40]. CDCs have been touted as promising for supercapacitors because carbide precursors allow the fine-tuning of porous networks [18,41] and better control over surface functional groups than activated carbons [42]. The porous network in CDCs can be tailored owing to the availability of varied distribution of carbon atoms in carbide precursors as well as by changing the synthesis temperature. To illustrate the first point, a comparison between titanium and silicon carbide derived carbons can be drawn, which shows that the same synthesis temperature of 1200 °C leads to the narrower pore size distribution and smaller average pore size of SiC-CDC [42]. The effect of the synthesis temperature reveals a common trend of increasing pore size with increasing synthesis temperature, independently of the precursors used [18,43]. It is worth noting that porous structure often collapses if the synthesis temperature exceeds 1300 °C whereas the graphitization of carbon occurs at temperatures higher than 1000 °C [44]. The properties of CDCs can be improved by post-treatment such as treatment with hydrogen [45].

CDCs' application to supercapacitors shows that the capacitance is governed by the CDC structure, whereas the rate performance depends significantly on starting carbide. Titanium CDCs was shown to have the highest gravimetric capacitance, up to 220 $F\ g^{-1}$ in KOH and 120 $F\ g^{-1}$ in organic electrolyte whereas SiC-CDC has the highest volumetric capacitance 126 $F\ cm^{-3}$ in KOH and 72 $F\ cm^{-3}$ in organic electrolyte [40]. In another work [46], the specific capacitance of TiC-CDC in an organic electrolyte using $(CH_3CH_2)_3CH_3NBF_4$ as a salt was found to be between 70 and 90 $F\ cm^{-3}$ or between 100 and 130 $F\ g^{-1}$ depending on the synthesis conditions.

A series of CDCs with tailored porosity prepared in the temperature range 600 °C–1200 °C were used to specifically study the effect of pore size, suggesting that pores narrower than 2 nm have a much larger effect on capacitance than the higher surface area CDCs with pores larger than 2 nm [18,47]. Another general trend derived from various studies on CDCs is that capacitance decreases with increasing the synthesis temperature despite the rise in the specific surface area and pore volume, again suggesting that pore size dominates capacitance value. CDC can also be adapted for either higher energy or higher power applications [48] by changing the synthesis temperature.

5.1.3. Carbon nanotubes (CNT)

Carbon nanotubes (CNTs) and carbon nanofibers, are produced by the catalytic decomposition of certain hydrocarbons [2,5]. It is possible to obtain different nanostructured formations controlling their crystalline order by manipulating different parameters [2]. Depending on the synthesis parameters, single walled carbon nanotubes (SWCNTs) and multi-walled carbon nanotubes (MWCNTs) can be prepared. These, have a fully accessible external surface area and high electric conductivity [2,5]. The specific capacitance of CNTs is greatly influenced by the purity and the morphology of the material [2]. The surface of CNT electrodes is mainly mesoporous, associated to the external face of the tubes [2]. Many research efforts are focused on the development of a dense and aligned, perpendicular to the current collector, CNT forest, which could increase the capacitance retention at high current by tuning the distance between tubes. This material seems to be promising for microelectronics applications [49,50].

CNTs can be grown in a conductive substrate without needing a binder. This minimizes the contact resistance between the active material and the current collector and simplifies electrode fabrication [51,52].

Mainly attributed to the hydrophobic property of CNT surface, the specific capacitance of purified CNT powders is in the range of 20 to 80 $F\ g^{-1}$ [49,2]. The specific capacitance can be increased by subsequent oxidative processes up to about 130 $F\ g^{-1}$. These oxidative treatments modify the surface texture and introduces additional surface functionality which is able to contribute to pseudocapacitance [53–55]. In [56] it catalytically grown MWCNTs of 8 nm diameter having a BET surface of about 250 $m^2\ g^{-1}$ were developed. CNTs were subsequently treated with nitric acid and formed into electrodes consisting of freestanding mats of entangled CNTs having an increased surface area of 430 $m^2\ g^{-1}$. This mat contained a negligible microporosity and an average pore diameter of 9.2 nm, which is 1.2 nm larger than the diameter of the nanotube itself. Much of the porosity in the nanotube mats is due to the interstitial spaces created by the entangled nanotube network. The specific capacitance in sulfuric acid was determined to be 102 $F\ g^{-1}$ at 1 Hz corresponding to a double layer of 24.2 $\mu F\ cm^{-2}$. This cell also had an estimated power density of more than 8 $kW\ kg^{-1}$.

Chemical activation of CNTs with potassium hydroxide can increase the surface-area maintaining the nanotubular morphology. These treatments have a negligible effect on nanotube diameter, but can considerably shorten their length and develop cracks and irregularities at the surface through a partial erosion of outer carbon layers. Using this activation, the BET surface-area of MWCNTs increased from 430 to 1035 $m^2\ g^{-1}$. This material maintained a high degree of mesoporosity, but microporosity was increased. The specific capacitance achieved was 90 $F\ g^{-1}$ (8.7 $\mu F\ cm^{-2}$) in alkaline media and 65 $F\ g^{-1}$ (6.2 $\mu F\ cm^{-2}$) in non-aqueous media [54].

50 nm diameter CNTs were grown on graphite foil, with a specific capacitance of 115.7 $F\ g^{-1}$ in 1 M H_2SO_4 and good

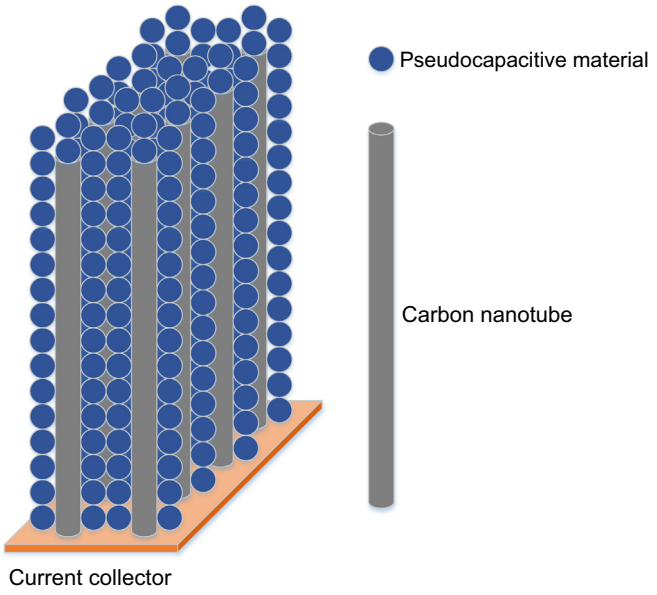

Fig. 8. Conformal deposit of pseudocapacitive material onto CNTs.

electrochemical stability [52]. Also, well aligned MWCNTs were grown on an aluminum film with lengths of 1–10 μm and diameters of 5–100 nm. This reached a volumetric capacitance of 120 F cm^{-3} and very high power density [51].

SWCNTs were also prepared as composites from polyvinylidene chloride (PVDC). After carbonization, the electrodes exhibited a maximum specific capacitance of 180 F g^{-1} and a measured power density of 20 kW kg^{-1} in potassium hydroxide [57]. This high specific capacitance for such a surface area of only 357 m^2 g^{-1} was attributed to a redistribution of CNT pore size to smaller and more optimal values of 3–5 nm [2].

As CNTs have limited SSA, leading to moderate capacitance, there is some interest in creating composites combining both CNTs and conducting polymers. These composites take advantage of the double layer capacitance of the CNTs and the pseudocapacitance of the conducting polymers, achieving higher capacitance than achievable with any of these materials alone. A graphical example in Fig. 8 illustrates a conformal deposit of pseudocapacitive material in CNTs. The composites are typically prepared by an in situ chemical polymerization of a suitable monomer, which usually forms a uniform coating on the CNT surface [2]. MWCNTs electrodeposited with polypyrrole (PPy) have achieved a specific capacitance of about 170 F g^{-1} [58,59], but due to the degradation of the polymer a cycle life greater than 100,000 cycles may not be achievable [60,61]. Similar composites using SWCNTs instead of MWCNTs have achieved specific capacitances up to 265 F g^{-1}. In these composites the PPy acts also as a conducting agent, thus reducing the ESR of the supercapacitor [2].

The degradation of these composites can be accelerated due to a possible overcharging/overdischarging during operation. In that case carbon-supported transition metal oxides can enhance stability [62]. Introducing a 1 wt% RuO_2 into MWCNT electrode can increase the specific capacitance from 30 to 80 F g^{-1}. Besides, it also exhibits longer cycle life than CNTs coated with a conducting polymer thin layer [62].

5.1.4. Graphene

Graphene is a one-atom thick sheet made of sp^2 bonded carbon atoms in a polyaromatic honeycomb crystal lattice [63–67]. This material is suitable for high performance energy storage systems due to their rate and cycle capability and improved capacity and excellent physiochemical properties [68]. Among the advantages of this material its large surface area, good flexibility, good electrical conductivity, good chemical and thermal stability, wide potential window and abundant surface functional groups can be highlighted [69].

Graphene based supercapacitors were reported with specific capacitance of 75 F g^{-1} and energy density of 31.9 W h kg^{-1} with ionic liquid electrolytes [70], and specific capacitances of 135 F g^{-1} in aqueous electrolyte and 99 F g^{-1} in organic electrolytes [71]. Reduced graphene with low agglomeration reached a maximum specific capacitance of 205 F g^{-1} in aqueous electrolyte exhibiting an energy density of 28.5 W h kg^{-1} [72].

It is difficult to determine the intrinsic capacitance of graphene because it exhibits a tendency to re-stack. A study reported that the intrinsic capacitance of the electric double layer in graphene is 21 μF cm^{-1} [73]. The interfacial capacitance of graphene depends on the number of layers, which can be calculated from the surface area. For graphene based supercapacitors in ionic liquids capable of operating up to 4.5 V, an energy density of 85.6 W h kg^{-1} is reached at room temperature, and 136 W h kg^{-1} at 80 °C [74].

The electrical conductivity of graphene is much higher than the one of graphitic carbon, and the theoretical surface area of a mono-layer is 2620 m^2 g^{-1}. It also has a high surface to volume ratio, short diffusion distance due to its thinness, structural flexibility, thermal and chemical stability, abundant surface functional groups, wide electrochemical window, and an open pore system which improves ion transport kinetics. On the other hand, this material suffers from irreversible capacity loss due to the re-stacking of the graphene sheets, which also reduces the initial Coulombic efficiency. This re-stacking occurs due to the van der Waals interaction between adjacent sheets, and reduces the surface area lowering its energy density [63].

To avoid the re-stacking of graphene sheets, composites made of graphene and metal oxides seem to be a good solution. This is beneficial for both materials because of their synergistic effect. Metal oxides prevent graphene from agglomeration and re-stacking, and also increase the available surface area. Besides, graphene helps the formation of metal oxide nanostructures with uniformly dispersed controlled morphologies, suppressing the volume change and agglomeration of metal oxides. The oxygen-containing groups within graphene will ensure good electrical contact, interfacial interactions, and bonding between graphene and metal oxide. This will lead to a composite with an electron conducting network and shortened ion paths [63]. In [75] different electrodes fabricated with graphene oxide are compared, achieving 352 F g^{-1} at 5 mV s^{-1} for three-dimensional porous network electrodes.

The experimentally obtained capacitance in graphene/metal oxide composites is higher than the sum of the calculated capacitances for each material individually. Also improvements in cycle capability, rate capability, energy density, and power density were reported for these composites owing to the integrated 3D structure. These enhancements in performance were also found in other non-metal oxide materials such as graphene nanosheets/polyaniline [76,77], graphene/$Co(OH)_2$ [78], graphene/$Ni(OH)_2$ [79], graphene/CNT [80], poly(sodium 4-styrensulfonate) intercalated graphene nanosheets [81], Pt-exfoliated graphene [82], carbon black supported graphene [83], and graphene/Si [84]. As examples the latest publications report exfoliated graphene with anchored polypyrrole reaching an energy density of 65.1 W h kg^{-1} at a power density of 13 kW kg^{-1}, and 82.4 W h kg^{-1} at 650 W kg^{-1} [85]. Ruthenium oxide-graphene hybrid material reached 479 F g^{-1} per hybrid material mass [86], and a graphene nanosheet-tungsten oxide composite was reported to reach 143.6 F g^{-1} [87].

Chemical doping of graphene with electron donors and acceptors is another way to improve the electrochemical properties of graphene-based electrodes. In [88] a N-doped graphene oxide supercapacitor was reported to reach 242 F g^{-1} with good

capacitance retention and cyclability. In [89] a capacitance of 320 F g^{-1} was reported for highly nitrogenated graphene oxide.

5.1.5. Mesoporous carbons

Mesoporous carbons can be prepared following different methods. Particularly, a high surface ordered meso-structures are interesting as they are capable of dealing with high power ratings without a significant capacity fading. Usually microporosity contains bottlenecks that can decrease ion mobility drastically, thus reducing the power capability of the electrode. Mesopores are not narrow paths slowing down the ion transport, so these can maintain capacitance even at high current densities.

There are several methods to synthesize mesoporous carbons: high-degree activation, carbonization of precursors composed of one thermosetting component and one thermally unstable component, catalyst-assisted activation of carbon precursors with metal oxides or organometallic compounds, or carbonization of aerogels or cryogels. These methods result in broad pore size distributions of mesoporous carbons, also exhibiting considerable microporosity [90]. Mesoporous carbons can also be synthesized using a replication synthesis with hard templates, and by self-assembly using soft templates through co-condensation and carbonization. These two methods are preferred because the pore size and distribution can be better controlled [90].

In hard template synthesis, templates serve as a mold with no significant chemical interactions between templates and carbon precursors, leading to well defined nanostructures. The soft template generates nanostructures through self-assembly of organic molecules. The pore structure is determined by synthetic conditions like, mixing ratios, solvents and temperature. These two methods have been proved as best suitable for the preparation of mesoporous structured carbons having a defined pore structure and narrow pore size distribution [90].

In [91] a mesoporous carbon obtained from lignin using Pluronic F127 surfactant is reported to achieve a SSA of 624 m^2 g^{-1} after CO_2 activation and a gravimetric specific capacitance up to 102 F g^{-1}. In [92] a mesoporous carbon using rice husk precursor is reported. This reaches a BET surface area of 1357 m^2 g^{-1} with a total pore volume of 0.99 ml g^{-1} and a 44.4% of mesoporosity. This carbon has a specific capacitance of 114 F g^{-1} in organic electrolyte at 5 mV s^{-1} scan rate.

5.2. Metal oxides

Metal oxides have high specific capacitance and conductivity, making them suitable for electrode fabrication focused on high energy and high power supercapacitors [4]. There are several different metal oxide materials used for electrode fabrication such as RuO_2 [93,94], IrO_2 [95], MnO_2 [96,97], NiO [98,99], Co_2O_3 [100], SnO_2 [101], V_2O_5 [102–104] or MoO_x [105,106]. The most studied ones are ruthenium and manganese oxides [8].

5.2.1. Ruthenium oxide

Ruthenium oxide (RuO_2) is one of the most explored electrode materials due to its advantages vis-a-vis other materials. This material has the highest specific capacitance among pseudocapacitive materials, about 1000 F g^{-1} [1]. Besides, it has a wide potential window, highly reversible redox reactions, high proton conductivity, good thermal stability, long cycle life, metallic-type conductivity, and high rate capability [107–110]. It also has three oxidation states accessible within 1.2 V [8,31]. But it has a very high cost [1], which reduces its applications to aerospace and military. The double layer capacitance only contributes to about 10% of the stored charge in RuO_2 electrodes, working in parallel with pseudocapacitance [8]. The pseudocapacitive behavior of ruthenium oxide involves different reactions in acidic and alkaline solutions [111,112]. In acidic electrolyte solutions, a fast reversible electron transfer and an electro-adsorption of protons onto the surface occurs where ruthenium oxidation states change from (II) to (IV) [113–117,111]:

$$RuO_2 + xH^+ + xe^- \leftrightarrow RuO_{2-x}(OH)_x \quad (11)$$

where $x \in [0 \ldots 2]$. The change of x during proton insertion/de-insertion occurs over 1.2 voltage window and leads to capacitive behavior due to ion adsorption following a Frumkin-type isotherm [117]. Specific capacitances above 600 F g^{-1} [118] have been achieved, but ruthenium-based aqueous systems are expensive, and their 1 V working voltage window limits their applications to small electronic devices [31]. In order to work with wider voltage windows, organic electrolytes with proton surrogates (for example $Li+$) must be used [31].

In alkaline solutions, it has been suggested that ruthenium is oxidized to RuO_4^{2-}, RuO_4^- and RuO_4 on charging and reduced back to RuO_2 on discharging [112,119].

Prototype cells developed by the US Army Research Lab were reported with an energy density of 8.5 W h kg^{-1} and power density of 6 kW kg^{-1} [120].

As charge storage comes mainly from pseudocapacitance of the surface on RuO_x, several attempts were made to increase electroactive surface, such as depositing RuO_2 films on substrates with rough surface, coating high surface areas with a thin RuO_2 film, or making nanometer-sized oxide electrodes [121–125]. Thus, a nanosized 3 nm hydrous RuO_2/carbon composite at a low loading of RuO_2 (10 to 20 wt %) achieved specific capacitances of 850–1200 F $g^{-1}_{RuO_2}$. As the content of ruthenium oxide increases, the specific capacitance in F g^{-1} of RuO_2 decreases due to low utilization by particle aggregation, at 50 wt.% of RuO_2 it was 288 F $g^{-1}_{RuO_2}$ [126].

Hydrous ruthenium oxide ($RuO_2 \cdot 0.5\ H_2O$) has a high specific capacitance of around 900 F g^{-1} [127] (theoretically 1358 F g^{-1} [28]) and high electrical conductivity 3×10^2 Ω^{-1} cm^{-1} [28]. This occurs because the inter-particle and inter-layer hydrous regions allow protonic conduction leading to a high power and high energy supercapacitor [128]. When the water content is decreased to $RuO_2 \cdot 0.3\ H_2O$ the capacitance drops down to 29 F g^{-1} and for anhydrous ruthenium oxide down to 0.5 F g^{-1} [127]. Amorphous hydrous ruthenium oxide prepared by sol–gel methods reaches a capacitance of 720 F g^{-1} [111,129]. Nevertheless, this value decreases at higher rates due to proton depletion and oversaturation in the electrolyte during cycling [130]. RuO_2xH_2O thin-film electrodes electrodeposited on a titanium substrate show highly reversible characteristics, excellent cycle stability, and good power capabilities, achieving a maximum electrode specific capacitance of 786 F g^{-1} [123]. Particles which are small, uniform in size, and highly dispersed on a carbon surface, prepared with the polyol method, exhibit a redox specific pseudocapacitance of 914 F g^{-1} [121]. Also specific capacitances of 1300 F g^{-1} were reported using nanotubular arrayed electrodes with hydrous ruthenium oxide [131].

The water content in ruthenium oxide depends strongly on the process followed for the preparation and the synthesis conditions. Usually only a fraction of chemically formed ruthenium oxide is active whereas electrolytically formed ruthenium oxide can have more hydrated oxide states for which more surface will be active in redox reactions. Typical water content x for a product dried at room temperature is 0.9, but dihydrated and trihydrated phases can also be obtained depending on the conditions [132]. Higher annealing temperature can result in a lack of chemically bound water, thus decreasing the specific capacitance [133,134].

The smaller size of a hydrated ruthenium oxide particle increases the gravimetric capacitance as this shortens the diffusion distance, facilitates the proton transport in the bulk, increases the

surface area, and enhances the electroactive sites. Thus, the particles should be nanosized to maintain high electrical and protonic conductivities throughout them [132,135]. If the nanopores are ordered, this enhances electrolyte diffusion into electrodes, improving the redox reaction and leading to higher pseudocapacitance [136].

The ionic concentration of the electrolyte should match the needs of the electrical double layer and the faradic reactions. In some electrolytes, pseudocapacitive behavior does not emerge regardless of the ruthenium oxide loading, but in other electrolytes pseudocapacitance is proportional to the RuO_x content [137,138].

As ruthenium oxide is too expensive, there are several studies focused on combining it with other low cost materials. For a SnO_2–RuO_2 composite electrode in which the ruthenium oxide was deposited with the incipient wetness precipitation method, a specific capacitance of 710 F g^{-1} was reported for a KOH electrolyte [112]. It is also reported that a RuO_2 (33%)–VO_2 (67%)/Ti electrode has a 50 times more specific charge than a RuO_2/Ti electrode [139]. Vanadium extends the potential window, and increases the utilization of ruthenium species and electrochemical stability [140]. Using TiO_2 nanotubes the utilization of RuO_2 is greatly enhanced [141]. Besides, double layer capacitance is enhanced, and TiO_2 facilitates the transport of ions [141].

5.2.2. Manganese oxide

Manganese oxides appear to be an alternative to RuO_2 thanks to their relatively low cost, low toxicity and environmental safety, and theoretical high capacitances going up to 1100–1300 F g^{-1} [142–145].

The main pseudocapacitive energy storage mechanism in this material is attributed to a reversible redox transitions involving the exchange of protons and/or cations with the electrolyte and transitions between different oxidation states, Mn(III)/Mn(II), Mn(IV)/Mn(III), and Mn(VI)/Mn(IV) [146,147]. This can be expressed using the following equation [8,142,146,148,149]:

$$MnO_\alpha(OC)_\beta + \delta C^+ + \delta e^+ \leftrightarrow MnO_{\alpha-\beta}(OC)_{\beta+\delta} \quad (12)$$

where C^+ represents the protons and alkali metal cations (Li^+, Na^+, K^+) in the electrolyte, and $MnO_\alpha(OC)_\beta$ and $MnO_{\alpha-\beta}(OC)_{\beta+\delta}$ are MnO_2nH_2O in high and low oxidation states, respectively.

Physical and chemical factors affect the pseudocapacitive behavior of manganese oxides [143,150,151]. Cycling stability is mainly controlled by the microstructure, whereas the specific capacitance is controlled mainly by the chemical hydrated state [152].

If the crystallinity of manganese oxide is too high, proton exchange will be limited as for ruthenium oxide. This will lead to a loss in surface area, but an increase in conductivity. If there is a low crystallinity, conductivity will decrease, so there must be a tradeoff between electrical conductivity and available surface area. As crystallinity is temperature dependent, heat-treated samples with an annealing temperature of 200 °C show a higher specific capacitance at high scan rates, and lower specific capacitance at low scan rates [153]. This is attributed to the lower surface area [8].

The morphology, composition and structures of MnO_x depend on the preparation conditions, affecting pseudocapacitive response in the material. The morphology of MnO_x is usually controllable by the preparation process or the reaction conditions [154]. For α-MnO_2 specific capacitances of 265–320 F g^{-1} were reported for the 0–1 V voltage window in a 0.1 M Na_2SO_4 aqueous electrolyte solution [146]. Specific capacitances of 195-275 F g^{-1} were achieved in 2 M KCl solution, and 310 F g^{-1} in 2 M $(NH_4)_2SO_4$ [146]. For γ-MnO_2 a specific capacitance of 240 F g^{-1} was achieved at 1 mA cm^{-2} [155], but usually the specific capacitances are in the range 20–30 F g^{-1} [156]. δ-MnO_2 synthesized in different ways exhibits specific capacitances of 236 F g^{-1} at 0.5 mA cm^{-2} in 0.1 M Na_2SO_4 electrolyte, but also specific capacitances exceeding 350 F g^{-1} [157,158] are reported.

In general, the specific capacitance of the material drops as the thickness of the electrode film is increased, as the result of the low conductivity characterizing MnO_2. For example, when the loading was increased from 50 to 200 μg cm^{-2} the specific capacitance dropped from 400 to 177 F g^{-1} [159]. Some benefits of using thin layers are the lower series resistance, and easy access of the electrolyte to the electrode [8], but the energy of the device will be lower due to the lower contribution of the thin film electrode to the overall mass/volume of the device as compared to thicker electrodes. Several MnO_2 thin film based systems were reported, reaching specific capacitances of about 600 F g^{-1} within potential windows going from 0.9 V until 1.2 V in aqueous electrolytes such as KCl, K_2SO_4, Na_2SO_4, and KOH [160,152,161–167].

As with ruthenium oxide, physically and chemically bonded water enhances the transport of electrolyte ions. This means that hydrated forms have better ion conductivity, thus exhibiting higher pseudocapacitance [168,169]. It was reported that heat-treatment above 200 °C removes all adsorbed water [143].

5.3. Polymers

Polymers electrodes have high electric conductivity, up to 10^4S cm^{-1} for doped polyacetylene, high electroactivity, which is the ability of an electrode coated with a polymer film to reversibly change its oxidation-reduction state in a solution under the application of an external electric field, the ability to form passive layers on metal surfaces, and the semiconductor band structure [170].

The typical cyclic voltammogram of a polymer electrode is not rectangular, as expected for a capacitor, but exhibits a current peak at redox potential of the polymer, while metal oxide electrodes can exhibit a series of redox reactions, giving an almost rectangular cyclic voltammogram shape. Regarding charge and discharge kinetics studied by cyclic voltammetry, devices made of these materials are battery-like. As a result the shape of a galvanostatic test is not triangular anymore, as expected for capacitors. An example of pseudocapacitor cycling is shown in Fig. 9 along with the shape obtainable from a capacitor.

These materials have reduced ESR and sometimes cost as compared to carbon materials. However the lack of efficient n-

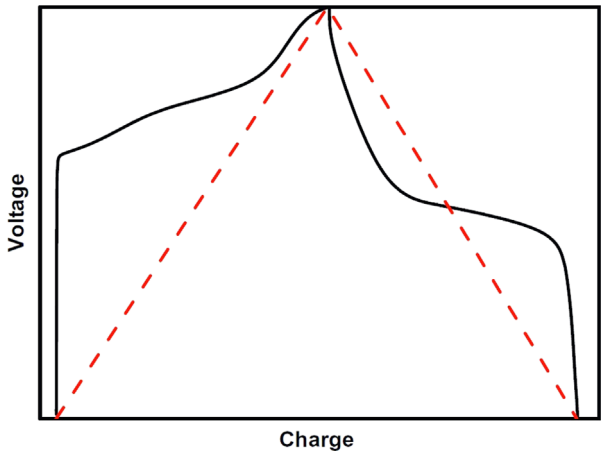

Fig. 9. Galvanostatic cycling with potential limitation of an ideal pseudocapacitor cell and a cell based on conducting polymers [187]. Cells using conducting polymers in black, ideal pseudocapacitor in dashed red. (For interpretation of the references to color in this figure caption, the reader is referred to the web version of this paper.)

doped conducting polymers makes it impossible to reach the same cell voltages found in carbon based cells [171,172].

Swelling and shrinking of polymers upon cycling can cause long term degradations [3,173,174]. Aromatic polyimides (PIs) are interesting as matrix for conducting composites because of their thermal stability, good mechanical properties and environmental stability. Composites made of intrinsically conducting polymers (ICPs) and PI matrix have improved mechanical properties, chemical stability and electrical properties under varying temperatures. For example, polypyrrole/polyimides (PPy/PI) composites show enhanced temperature and environmental stability [170]. The excellent miscibility between PPy carbonyls and PI's NH is caused by hydrogen bonding. This composite has also an excellent electroactivity [175].

A thin (less than 100 μm) high surface area conducting polymer can be grown on a current collector in order to make an electrode. During this electrochemical formation process the electrode can be p-doped or n-doped. On charging or discharging the electrode the dopant ions move in or out of the polymer electrode forming an electric double layer. These materials' charging mechanism is claimed to be pseudocapacitive rather than double layer charging, reaching very high capacitances (400–500 F g^{-1} of active material if the surface area is large enough) [170].

PPy is electroactive at positive electrode potentials [170]. PIs are electroactive at negative potentials, and under certain conditions also at positive potentials [175]. This makes it possible to use PPy/PI composites for supercapacitors.

6. Electrolytes

The electrolyte also plays an important role in the supercapacitor performance. The electrolyte concentration has to be high so as to avoid depletion problems during the charge of the supercapacitor, especially for organic electrolyte ("the electrolyte starvation effect") [176]. If the electrolyte reservoir is too small as compared to the large electrode surface the performance of a supercapacitor cell will be reduced. Concentrations higher than 0.2 molar are normally sufficient [3].

Most important properties to take into account in electrolytes are the temperature coefficient and the conductivity, which mainly determines the ESR of a supercapacitor. Other requirements include a wide voltage window, high electrochemical stability, high ionic concentration, low solvated ionic radius, low viscosity, low volatility, low toxicity, low cost, and availability at high purity [8]. The specific conductivity of a solution can be empirically optimized by means of choosing mixed solvents, modifying thus the solvation of the ions and the viscosity of the solution. Besides, the thermodynamic potential range of electrochemical stability is very important, being higher for non-aqueous electrolytes than for aqueous solutions. The corrosion of electrodes and current collectors is important as well. This depends on the nature of electrolytes, and for aqueous electrolytes on the pH. A preliminary study on the potential range of safe and reversible operation for any material/electrolyte couple is needed to ensure the viability of final systems.

6.1. Aqueous and organic electrolytes

Electrolytes widely used in supercapacitors can be classified as aqueous and organic. Aqueous electrolytes have limited their cell voltage typically to 1 V due to the water decomposition at 1.23 V, whereas cells based on organic electrolytes can reach voltages of 2.7 V and higher [8]. Nevertheless organic electrolytes exhibit at least 20 times higher specific resistance than aqueous ones, typically a 50 times higher specific resistance [3], which leads to a reduced power capability. The conductivity of aqueous electrolytes is about 1 S cm^{-1} [2]. Aqueous electrolytes also have lower minimum pore size requirements compared to organic electrolytes [177]. Aqueous electrolytes can also provide more capacitance than organic electrolytes due to higher concentration and smaller ionic radius [8].

Regarding industrial production, organic electrolytes are more expensive due to the purification from water, which is needed to provide the higher cell voltage without degrading the electrolyte [3]. Water content should be kept below 3–5 ppm in organic electrolytes [8].

Among organic electrolytes, the most widely used solvents are acetonitrile (ACN) and propylene carbonate (PC). ACN is capable of dissolving larger amounts of salts, but is toxic, while PC-based electrolytes are more environmentally friendly, offering a wide working voltage, wide working temperature, and lower but relatively good conductivity [8]. Among the salts used in organic electrolytes, tetraethylammonium tetrafluoroborate, tetraethylphosphonium tetrafluoroborate, and triethylmethylammonium tetrafluoroborate can be found. The salts exhibiting less symmetric structures have lower crystal lattice energy, therefore increased solubility [8].

6.2. Ionic liquids

Low-temperature ionic liquids (ILs), which are the type of ILs of interest to supercapacitors, are pure organic salts containing no solvents with melting points below 100 °C. If the liquid state in maintained at ambient temperature, they are termed room temperature ionic liquids (RTILs). RTILs are of interest to supercapacitors because they are nonvolatile, poorly combustible, and heat-resistant, with these properties being very peculiar and unachievable with conventional solvents. In RTILs, at least one ion usually has a delocalized charge (very often aromatic structures) and one component is organic, which prevents the formation of a stable crystal lattice. Properties such as melting point, viscosity, and conductivity are controlled by both the substituents on the organic ion and by the counterion. Many ionic liquids can be and have been developed with the extensive variation of physicochemical properties. For this reason, ionic liquids have been termed "designer solvents".

Ionic liquid gel polymer electrolytes (ILGPEs) are also developed by incorporating ionic liquids into a polymer matrix. These are mechanically strong, electrochemically and thermally stable, and highly conductive.

Ionic liquids are resistant to the reduction and the oxidation in a wide voltage potential window, which depends on the counter ion, providing a cell voltage of around 4.5 V, with some of them being able to reach 6 V [178]. Since ILs are solvent free, as shown in Fig. 2 there is no solvation shell, so the ion size is better known [19]. The most important properties of ionic liquids from the point of view of the electrochemistry are, conductivity, viscosity, and the potential range of electrochemical stability. The main drawback of IL electrolytes is their low electrical conductivity, which is typically less than 10 mS cm^{-1} [178], and is significantly lower compared to aqueous electrolytes. The conductivity of ionic liquids is strongly correlated to their viscosity, with strong temperature dependence [179]. In order to overcome the low conductivity, a dilution with organic solvents is sometimes applied [8]. Some ILs have a reasonably good ionic conductivity, comparable to the best organic solvent electrolytes [179].

Also a good electrode structure is needed to assure the proper wettability by the electrolyte [180].

The classical EDL theories in aqueous electrolytes and high-temperature molten salts are not expected to describe accurately the structure and properties of EDLs forming between ionic liquids and electrified surfaces. Experimental data suggest that the

thickness of the EDL between ionic liquid and electrode is of one ion layer (typically 3–5 Å). This supports that EDLs in ionic liquids are essentially the Helmholtz layers.

Preliminary results demonstrate that the ionic liquids are a good solution to improve the performance of electrochemical capacitors, particularly for temperatures in fuel-cell vehicle applications [179]. On the other hand, ILs often have prohibitive cost and require more stringent conditions for drying carbon materials in order to provide water-free environments in the cells. As of today, these are major impediments to the industrial use of ILs as supercapacitor electrolyte. Another issue with ILs is poor compatibility with microporous carbons.

7. Electrochemical configuration of supercapacitor cells

The electrochemical configuration of supercapacitor cells is detailed in Fig. 3, which shows that supercapacitors can be symmetric or asymmetric. Typically, the symmetric supercapacitors are made up of two identical carbon electrodes, schematically shown in Fig. 4.

The asymmetric supercapacitors are fabricated with different electrodes. This can be two electrodes made of the same carbons but having different thicknesses (masses) or two different carbons, or a pseudocapacitive material in at least one electrode. A more distinct type of supercapacitor cells are hybrid cells (so-called internal hybrids [181]), combining the non-Faradaic and Faradaic battery-type behavior in a single cell. These can be broken down into internal series hybrids (ISHs) and internal parallel hybrids (IPHs). In the case of ISH, one electrode is a battery-type electrode, ideally working at a constant potential and being limited by a slow diffusion-process with a high charge storage capacity whereas the other is a capacitive electrode exhibiting a sloppy potential profile typical of a supercapacitor. A representative example of such a commercial system is the LiC. By contrast, an IPH combines battery and capacitive materials at each electrode, providing higher energy at low current, but also being able to operate at a current non-typically high for battery materials because of the presence of a capacitive material in the electrode. These systems provide higher energy owing to the higher operating voltage and higher capacity than symmetric systems as explained below.

Commercially available hybrid devices with specific energies exceeding 10 W h kg^{-1} can be found, which are suitable for traction applications with charge times of about 10 minutes [1]. The rated voltage (U_r) of these devices is given as the difference between the potentials of the positive (ΔE_+) and the negative electrodes (ΔE_-). $U_r = \Delta E_+ - \Delta E_-$. The amount of charge accumulated on both electrodes is identical, $Q_+ = \Delta E_+ C_+ = \Delta E_- C_- = Q_-$. Since one of the electrodes in an ISH has much higher capacitance, the potential range of the other electrode is higher [182]. The use of a non-polarizable electrode raises the voltage of the single cell, and, since the second capacitive electrode of a symmetric capacitor is removed, the total capacity increases. This changes increases in 2–5 times the specific energy comparing to symmetric designs [183]. Since the self-discharge of an EDLC it is basically only due to the capacitive carbon electrode, the asymmetric types have lower self-discharge than symmetric ones. However, the service life is reduced due to the cycling of the Faradaic (non-polarizable) electrode. It is important to make the right choice of capacities ratio to reduce the depth of discharge of the Faraday electrode [183]. The discharge time constant is larger in this type of devices. This occurs due to a high inertness of the asymmetric systems because of a relatively slow electrochemical reaction in the non-polarizable electrode. For example, one of the fastest electrochemical reactions, a proton exchange in a solid phase, is still slower than the process of electric double-layer formation on the phase boundary solid/electrolyte. Therefore the discharge time constant of a series-produced asymmetric EC, is higher, typically more than 1 s [183].

7.1. Lithium-ion capacitors

LiCs are a kind of advanced asymmetric energy storage devices. These systems have functionalities derived from both batteries and conventional EDLCs, and are capable of storing 5–10 times more energy than conventional EDLCs. These devices are high power and long cycle-life energy storage systems [184].

The typical LiC is built with a high surface area activated carbon as the positive electrode, and an intercalation compound, which supports fast reversible intercalation of lithium ions, as the negative electrode.

During the charge of a LiC, lithium ion intercalation proceeds inside the bulk of the negative electrode, while anion adsorption occurs onto the surface of the positive electrode. During discharge, lithium ion deintercalation occurs from the bulk of the negative electrode, while anion desorption takes place on the surface of the activated carbon positive electrode. As the process on the positive electrode is non-faradaic, it is faster in comparison with the lithium-ion exchange process in the negative electrode. This means that the power density of the device will be determined by the rate capability of the negative electrode [184].

There are various materials evaluated as negative electrodes, all of them in non-aqueous electrolytes: Nanostructured $Li_4Ti_5O_{12}$ (LTO), disordered or semi-crystalline graphite, graphite, pre-lithiated graphitic carbon, Li_2FeSiO_4. Fig. 10 shows the voltage profile for graphite/AC and LTO/AC cells, comparing them to EDLCs.

There are also configurations using activated carbon as a negative electrode. These devices have lower cell voltages due to

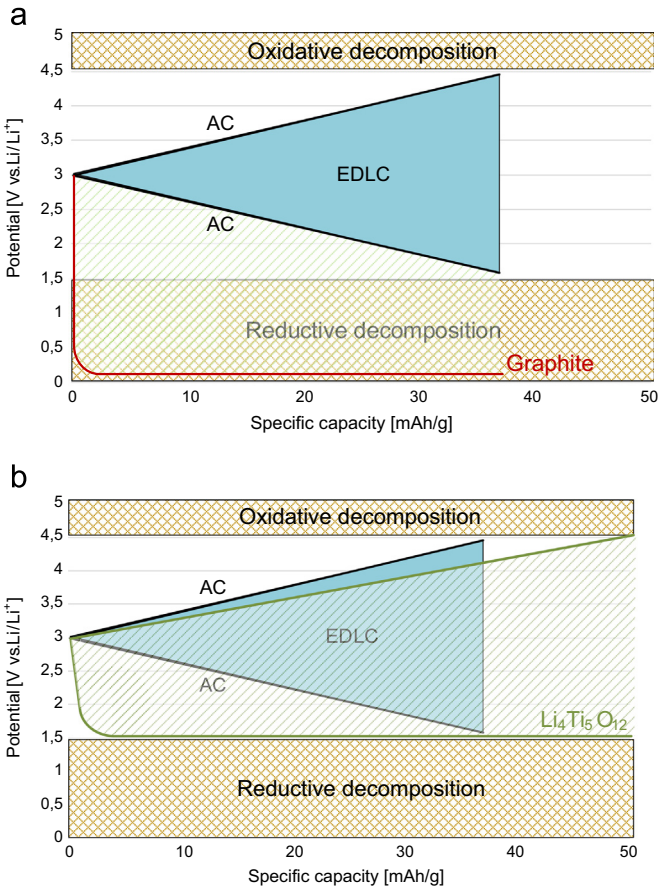

Fig. 10. Typical voltage profiles for LiC cell (a) and LTO-CNF/AC cell (b) compared to a symmetric EDLC cell.

limited operating potential windows of the electrodes in such arrangement. The positive electrodes can be made of graphite or $LiNi_{0.5}Mn_{1.5}O_4$.

Partially disordered graphitic carbons have lower redox potential than LTO, ideally providing higher voltage and higher energy. Cells assembled with negative graphitic carbon electrodes have a wider operating voltage range and an improved energy density. Using disordered carbon or semi-crystalline graphitic materials, the lithium-ion intercalation/de-intercalation process can occur over a wide voltage range, which leads to a steep decrease in cell voltage during discharge and a corresponding decrease in the energy density. Ordered graphite has a relatively flat lithium intercalation/deintercalation profile at low negative redox potential. However, graphite-based cells, suffer from slow kinetics during initial charging cycles. The pre-lithiation of the graphite anode is achieved by using an additional internal lithium metal electrode. Pre-lithiation is needed for the following reasons: (i) it enables high voltage (about 4 V) without excess charging, (ii) it suppresses the irreversible capacity of the negative electrode, (iii) it reduces electrode resistance, (iv) it reduces Li^+ consumption from the electrolyte, (v) it extends cycle-life and (vi) it provides high energy density through the extended potential swing of positive electrode.

The LTO/acetonitrile/activated carbon (AC) system was one of the first to achieve an energy density of 10 W h kg^{-1} at 3.2 V with good power capability [28]. Devices with working voltages up to 3.8 V have achieved energy densities of 25 W h kg^{-1} [28]. The volumetric energy densities reach 30 W h l^{-1} [28].

Further development of this technology is needed before commercialization to avoid the accumulation of solid electrolyte interface on negative electrodes, and improve the cycling performances and ensure safety [28].

8. Manufacturers

The number of supercapacitor developer and manufacturers is growing rapidly. Most of the market is taken by organic-based supercapacitors using acetonitrile or propylene carbonate-based electrolytes, but nowadays near the 50% of the available manufacturers offer devices based on non-flammable and relatively non-toxic electrolytes, which is an advantage.

There are several applications in which a supercapacitor can be the best solution, and these applications differ from each other in terms of requirements for the ESS.

Table 4 summarizes different manufacturers and some of their products targeted to high power applications. The table includes typical specifications, and also energy and power densities. In the case of power densities two values are included, the one for the highest achievable power density, which is related to the power given with a matched impedance, and the other related to a working efficiency of 95%.

Table 4
Different products offered by manufacturers. Data taken from [5].

Manufacturer	V	C (F)	ESR (mΩ)	W h kg^{-1}	W kg^{-1} (95%)	W kg^{-1} (Matched)
Maxwell	2.7	2800	0.48	4.45	900	8000
Apowercap	2.7	590	0.9	5	2618	23,275
Nesscap	2.7	1800	0.55	3.6	975	8674
Nesscap	2.7	5085	0.24	4.3	958	8532
Asahi Glass (PC)	2.7	1375	2.5	4.9	390	3471
Panasonic (PC)	2.5	1200	1	2.3	514	4596
LS Cable	2.8	3200	0.25	3.7	1400	12,400
BatScap	2.7	1680	0.2	4.2	2050	18,225
Power Sys (PC)	2.7	1350	1.5	4.9	650	5785

9. Conclusions

Supercapacitors are a very interesting technology for different applications requiring high power ratings, long cycle and calendar life, and reliability. Those requirements are stipulated by renewable energy systems such as wind power conversion and solar systems. The first requires high power burst for blade-pitch adjusting or enhancing low voltage ride-through capability. The second requires output power smoothing, which is classically done with the batteries that do not last more than few years [182].

In this review we gathered different electrode and electrolyte materials, pointing out their advantages and disadvantages in supercapacitors. We particularly note that special care must be taken to provide a good electrode–electrolyte match in order to achieve good capacitance ratings. Optimizing the electrode–electrolyte interface is crucial for maximizing performance, especially capacitance and rate capability of supercapacitors.

A proper material selection must be done taking into account the requirements from final application such as cycle life, specific energy and powers, energy and power densities and calendar life. Apart from the materials, the design and optimization of new cell configurations is a growing field of opportunities for developing hybrid battery/supercapacitor systems. Such systems will be in great demand in those applications where a battery or supercapacitor alone does not meet specific needs such as energy density, cycle life, and power rating.

Equally important to the material and cell development is the processing of electrodes and cell assembly, which should be optimized to maximize the performance.

Finally, we note on the application side that in most of the cases supercapacitors are used complementarily to batteries, being able to enhance their operating efficiency as well as the overall performance of an ESS.

References

[1] Miller JR, Simon P. Electrochemical capacitors for energy management. Science 2008;321(5889):651–2. https://dx.doi.org/10.1126/science.1158736 URL <https://www.sciencemag.org/content/321/5889/651.full>.
[2] Pandolfo A, Hollenkamp A. Carbon properties and their role in supercapacitors. J Power Sources 2006;157(1):11–27. http://dx.doi.org/10.1016/j.jpowsour.2006.02.065 URL ⟨http://linkinghub.elsevier.com/retrieve/pii/S0378775306003442⟩.
[3] Kötz R, Carlen M. Principles and applications of electrochemical capacitors. Electrochim Acta 2000;45:2483–98 URL ⟨http://www.sciencedirect.com/science/article/pii/S0013468600003546⟩.
[4] Sharma P, Bhatti T. A review on electrochemical double-layer capacitors. Energy Convers Manag 2010;51(12):2901–12. http://dx.doi.org/10.1016/j.enconman.2010.06.031 URL ⟨http://linkinghub.elsevier.com/retrieve/pii/S0196890410002438⟩.
[5] Simon P, Burke A. Nanostructured carbons: double-layer capacitance and more. Electrochem. Soc. Interface 2008;17(1):38–44. URL ⟨http://www.electrochem.org/dl/interface/spr/spr08/spr08_p38-43.pdf⟩.
[6] Portet C, Taberna P, Simon P, Laberty-Robert C. Modification of Al current collector surface by sol–gel deposit for carbon–carbon supercapacitor applications. Electrochim Acta 2004;49(6):905–12. http://dx.doi.org/10.1016/j.electacta.2003.09.043 URL ⟨http://www.sciencedirect.com/science/article/pii/S0013468603007928⟩.
[7] Gogotsi Y, Presser V. Carbon nanomaterials. 2nd edition.. Boca Raton, Florida: CRC Press; 2013.
[8] Wang G, Zhang L, Zhang J. A review of electrode materials for electrochemical supercapacitors. Chem Soc Rev 2012;41(2):797–828. http://dx.doi.org/10.1039/c1cs15060j URL ⟨http://www.ncbi.nlm.nih.gov/pubmed/21779609⟩.
[9] Endo M, Takeda T, Kim Y, Koshiba K, Ishii K. High power electric double layer capacitor (EDLC's); from operating principle to pore size control in advanced activated carbons. Carbon Sci 2001;1(3):117–28 URL ⟨http://carbonlett.org/Upload/files/CARBONLETT/117-128.pdf⟩.

[10] Bagotsky V. Fundamentals of electrochemistry. Hoboken, New Jersey: John Wiley & Sons, Inc.; 2005.

[11] Zhang LL, Zhao XS. Carbon-based materials as supercapacitor electrodes. Chem Soc Rev 2009;38(9):2520–31. http://dx.doi.org/10.1039/b813846j URL ⟨http://www.ncbi.nlm.nih.gov/pubmed/19690733⟩.

[12] Barbieri O, Hahn M, Herzog A, Kötz R. Capacitance limits of high surface area activated carbons for double layer capacitors. Carbon 2005;43(6):1303–10. http://dx.doi.org/10.1016/j.carbon.2005.01.001 URL ⟨http://www.sciencedirect.com/science/article/pii/S0008622305000047⟩ http://linkinghub.elsevier.com/retrieve/pii/S0008622305000047⟩.

[13] Qu D, Shi H. Studies of activated carbons used in double-layer capacitors. J Power Sources 1998;74(1):99–107. http://dx.doi.org/10.1016/S0378-7753(98)00038-X URL ⟨http://www.sciencedirect.com/science/article/pii/S037877539800038X, http://linkinghub.elsevier.com/retrieve/pii/S037877539800038X⟩.

[14] Gamby J, Taberna P, Simon P, Fauvarque J, Chesneau M. Studies and characterisations of various activated carbons used for carbon/carbon supercapacitors. J Power Sources 2001;101(1):109–16. http://dx.doi.org/10.1016/S0378-7753(01)00707-8 URL ⟨http://www.sciencedirect.com/science/article/pii/S0378775301007078, http://linkinghub.elsevier.com/retrieve/pii/S0378775301007078⟩.

[15] Shi H. Activated carbons and double layer capacitance. Electrochim Acta 1996;41(10):1633–9. http://dx.doi.org/10.1016/0013-4686(95)00416-5 URL ⟨http://www.sciencedirect.com/science/article/pii/0013468695004165⟩.

[16] Qu D. Studies of the activated carbons used in double-layer supercapacitors. J Power Sources 2002;109(2):403–11. http://dx.doi.org/10.1016/S0378-7753(02)00108-8 URL ⟨http://www.sciencedirect.com/science/article/pii/S0378775302001088⟩.

[17] Kim Y, Horie Y, Ozaki S, Matsuzawa Y, Suezaki H, Kim C, et al. Correlation between the pore and solvated ion size on capacitance uptake of PVDC-based carbons. Carbon 2004;42(8–9):1491–500. http://dx.doi.org/10.1016/j.carbon.2004.01.049 URL ⟨http://www.sciencedirect.com/science/article/pii/S0008622304000594⟩.

[18] Chmiola J, Yushin G, Gogotsi Y, Portet C, Simon P, Taberna PL. Anomalous increase in carbon capacitance at pore sizes less than 1 nanometer. Science (New York, N.Y.) 2006;313(5794):1760–3. http://dx.doi.org/10.1126/science.1132195 URL ⟨http://www.ncbi.nlm.nih.gov/pubmed/16917025⟩.

[19] Largeot C, Portet C. Relation between the ion size and pore size for an electric double-layer capacitor. J Am Chem Soc 2008;130(9):2730–1. http://dx.doi.org/10.1021/ja7106178 URL ⟨http://pubs.acs.org/doi/abs/10.1021/ja7106178⟩.

[20] García-Gómez A, Moreno-Fernández G, Lobato B, Centeno Ta. Constant capacitance in nanopores of carbon monoliths. Phys Chem Chem Phys 2015;17(24):15687–90. http://dx.doi.org/10.1039/C5CP01904D URL ⟨http://xlink.rsc.org/?DOI=C5CP01904D⟩.

[21] Stoeckli F, Centeno TA. Pore size distribution and capacitance in microporous carbons. Phys Chem Chem Phys 2012;14(33):11589–91. http://dx.doi.org/10.1039/C2CP41545C URL ⟨http://dx.doi.org/10.1039/C2CP41545C⟩.

[22] Centeno Ta, Stoeckli F. The volumetric capacitance of microporous carbons in organic electrolyte. Electrochem Commun 2012;16(1):34–6. http://dx.doi.org/10.1016/j.elecom.2011.12.017.

[23] Vix-Guterl C, Frackowiak E, Jurewicz K, Friebe M, Parmentier J, Béguin F. Electrochemical energy storage in ordered porous carbon materials. Carbon 2005;43(6):1293–302. http://dx.doi.org/10.1016/j.carbon.2004.12.028.

[24] Huang J, Sumpter B, Meunier V. Theoretical model for nanoporous carbon supercapacitors. Angew Chem 2008;120(3):530–4. http://dx.doi.org/10.1002/ange.200703864 URL ⟨http://doi.wiley.com/10.1002/ange.200703864⟩.

[25] Feng G, Qiao R, Huang J, Sumpter BG, Meunier V. Ion distribution in electrified micropores and its role in the anomalous enhancement of capacitance. ACS Nano 2010;4(4):2382–90. http://dx.doi.org/10.1021/nn100126w.

[26] Augustyn V, Simon P, Dunn B. Pseudocapacitive oxide materials for high-rate electrochemical energy storage. Energy Environ Sci 2014;7(5):1597–614. http://dx.doi.org/10.1039/C3EE44164D.

[27] Conway BE, Pell WG. Double-layer and pseudocapacitance types of electrochemical capacitors and their applications to the development of hybrid devices. J Solid State Electrochem 2003;7(9):637–44. http://dx.doi.org/10.1007/s10008-003-0395-7.

[28] Naoi K, Simon P. New materials and new configurations for advanced electrochemical capacitors. Electrochem. Soc. Interface 2008;17(1):34–7. URL ⟨http://www.electrochem.org/dl/interface/spr/spr08/spr08_p38-43.pdf⟩.

[29] Chuang C-M, Huang C-W, Teng H, Ting J-M. Effects of carbon nanotube grafting on the performance of electric double layer capacitors. Energy Fuels 2010;24(12):6476–82. http://dx.doi.org/10.1021/ef101208x URL ⟨http://pubs.acs.org/doi/abs/10.1021/ef101208x⟩.

[30] Zhu ZZ, Wang GC, Sun MQ, Li XW, Li CZ. Fabrication and electrochemical characterization of polyaniline nanorods modified with sulfonated carbon nanotubes for supercapacitor applications. Electrochim Acta 2011;56(3):1366–72. http://dx.doi.org/10.1016/j.electacta.2010.10.070.

[31] Simon P, Gogotsi Y. Materials for electrochemical capacitors. Nat Mater 2008;7(11):845–54. http://dx.doi.org/10.1038/nmat2297 URL ⟨http://www.ncbi.nlm.nih.gov/pubmed/18956000⟩.

[32] Jurewicz K, Vix-Guterl C. Capacitance properties of ordered porous carbon materials prepared by a templating procedure. J Phys Chem Solids 2004;65:287–93. http://dx.doi.org/10.1016/j.jpcs.2003.10.024 URL ⟨http://www.sciencedirect.com/science/article/pii/S0022369703003858⟩.

[33] Fernández J, Morishita T, Toyoda M. Performance of mesoporous carbons derived from poly (vinyl alcohol) in electrochemical capacitors. J Power … 2008;175(2008):675–9. http://dx.doi.org/10.1016/j.jpowsour.2007.09.042 URL ⟨http://www.sciencedirect.com/science/article/pii/S0378775307020083⟩.

[34] Jiang J, Zhang L, Wang X, Holm N, Rajagopalan K, Chen F, et al. Highly ordered macroporous woody biochar with ultra-high carbon content as supercapacitor electrodes. Electrochim Acta 2013;113:481–9. http://dx.doi.org/10.1016/j.electacta.2013.09.121 URL ⟨http://linkinghub.elsevier.com/retrieve/pii/S0013468613018859⟩.

[35] Du X, Zhao W, Wang Y, Wang C, Chen M, Qi T, et al. Preparation of activated carbon hollow fibers from ramie at low temperature for electric double-layer capacitor applications. Bioresour Technol 2013;149:31–7. http://dx.doi.org/10.1016/j.biortech.2013.09.026 URL ⟨http://www.ncbi.nlm.nih.gov/pubmed/24084201⟩.

[36] Thambidurai A, Lourdusamy JK, John JV, Ganesan S. Preparation and electrochemical behaviour of biomass based porous carbons as electrodes for supercapacitors a comparative investigation. Kor J Chem Eng 2014;31(2):268–75. http://dx.doi.org/10.1007/s11814-013-0228-z URL ⟨http://link.springer.com/10.1007/s11814-013-0228-z⟩.

[37] Wei L, Yushin G. Nanostructured activated carbons from natural precursors for electrical double layer capacitors. Nano Energy 2012;1(4):552–65. http://dx.doi.org/10.1016/j.nanoen.2012.05.002 URL ⟨http://linkinghub.elsevier.com/retrieve/pii/S2211285512001097⟩.

[38] Ersoy DA, McNallan MJ, Gogotsi Y. Carbon coatings produced by high temperature chlorination of silicon carbide ceramics. Mater Res Innov 2001;5(2):55–62. http://dx.doi.org/10.1007/s100190100136 URL ⟨http://link.springer.com/10.1007/s100190100136⟩.

[39] Gogotsi YG, Jeon I-D, McNallan MJ. Carbon coatings on silicon carbide by reaction with chlorine-containing gases. J Mater Chem 1997;7(9):1841–8. http://dx.doi.org/10.1039/a701126a.

[40] Cambaz ZG, Yushin GN, Gogotsi Y, Vyshnyakova KL, Pereselentseva LN. Formation of carbide-derived carbon on β-silicon carbide whiskers. J Am Ceram Soc 2006;89(2):509–14. http://dx.doi.org/10.1111/j.1551-2916.2005.00780.x.

[41] Gogotsi Y, Nikitin A, Ye H, Zhou W, Fischer JE, Yi B, et al. Nanoporous carbide-derived carbon with tunable pore size. Nat Mater 2003;2(9):591–4. http://dx.doi.org/10.1038/nmat957.

[42] Yushin G, Nikitin A, Gogotsi Y. Carbide derived carbon. In: Gogotsi Y, editor. Nanomaterials handbook. Boca Raton, FL: CRC Press; 2006. p. 237–80.

[43] Dash R, Chmiola J, Yushin G, Gogotsi Y, Laudisio G, Singer J, et al. Titanium carbide derived nanoporous carbon for energy-related applications. Carbon 2006;44(12):2489–97. http://dx.doi.org/10.1016/j.carbon.2006.04.035.

[44] Kravchik AE, Kukushkina JA, Sokolov VV, Tereshchenko GF. Structure of nanoporous carbon produced from boron carbide. Carbon 2006;44(15):3263–8. http://dx.doi.org/10.1016/j.carbon.2006.06.037.

[45] Erdemir A, Kovalchenko A, McNallan MJ, Welz S, Lee A, Gogotsi Y, et al. Effects of high-temperature hydrogenation treatment on sliding friction and wear behavior of carbide-derived carbon films. Surface and coatings technology 2004;188–189(1–3 Spec. Iss.):588–93. http://dx.doi.org/10.1016/j.surfcoat.2004.07.052.

[46] Permann L, Lätt M, Leis J, Arulepp M. Electrical double layer characteristics of nanoporous carbon derived from titanium carbide. Electrochim Acta 2006;51(7):1274–81. http://dx.doi.org/10.1016/j.electacta.2005.06.024.

[47] Chmiola J, Yushin G, Dash R, Gogotsi Y. Effect of pore size and surface area of carbide derived carbons on specific capacitance. J Power Sources 2006;158(1):765–72. http://dx.doi.org/10.1016/j.jpowsour.2005.09.008.

[48] Taberna PL, Simon P, Fauvarque JF. Electrochemical characteristics and impedance spectroscopy studies of carbon–carbon supercapacitors. J Electrochem Soc 2003;150(3):A292–300. http://dx.doi.org/10.1149/1.1543948 URL ⟨http://jes.ecsdl.org/content/150/3/A292.abstract⟩.

[49] Talapatra S, Kar S, Pal SK, Vajtai R, Ci L, Victor P, et al. Direct growth of aligned carbon nanotubes on bulk metals. Nat Nanotechnol 2006;1(2):112–6. http://dx.doi.org/10.1038/nnano.2006.56 URL ⟨http://www.ncbi.nlm.nih.gov/pubmed/18654161⟩.

[50] Pushparaj VL, Shaijumon MM, Kumar A, Murugesan S, Ci L, Vajtai R, et al. Flexible energy storage devices based on nanocomposite paper. Proc Natl Acad Sci 2007;104(34):13574–7.

[51] Emmenegger C, Mauron P, Züttel A. Carbon nanotube synthesized on metallic substrates. Appl Surf Sci 2000:452–6 URL ⟨http://www.sciencedirect.com/science/article/pii/S0169433200002324⟩.

[52] Chen J, Li W, Wang D, Yang S, Wen J, Ren Z. Electrochemical characterization of carbon nanotubes as electrode in electrochemical double-layer capacitors. Carbon 2002;40:1193–7 URL ⟨http://www.sciencedirect.com/science/article/pii/S0008622301002664⟩.

[53] Frackowiak E, Béguin F. Carbon materials for the electrochemical storage of energy in capacitors. Carbon 2001;39(6):937–50. http://dx.doi.org/10.1016/S0008-6223(00)00183-4 URL ⟨http://linkinghub.elsevier.com/retrieve/pii/S0008622300001834⟩.

[54] Frackowiak E, Delpeux S, Jurewicz K, Szostak K. Enhanced capacitance of carbon nanotubes through chemical activation. Chem Phys Lett 2002;361(July):35–41.

[55] Frackowiak E, Metenier K, Bertagna V, Beguin F. Supercapacitor electrodes from multiwalled carbon nanotubes. Appl Phys Lett 2000;77(15):2421. http://dx.doi.org/10.1063/1.1290146 URL ⟨http://link.aip.org/link/APPLAB/v77/i15/p2421/s1&Agg=doi⟩.

[56] Niu C, Sichel EK, Hoch R, Moy D, Tennent H. High power electrochemical capacitors based on carbon nanotube electrodes. Appl Phys Lett 1997;70 (11):1480. http://dx.doi.org/10.1063/1.118568 URL ⟨http://link.aip.org/link/APPLAB/v70/i11/p1480/s1&Agg=doi⟩.

[57] Choi YC, Lee SM, Chung DC. Supercapacitors using single-walled carbon. Adv Mater 2001;13(7):497–500.

[58] Hughes M, Shaffer MSP, Renouf AC, Singh C, Chen GZ, Fray DJ, et al. Electrochemical capacitance of nanocomposite films formed by coating aligned arrays of carbon nanotubes with polypyrrole. Adv Mater 2002;14(5):382–5.

[59] Frackowiak E, Jurewicz K, Szostak K, Delpeux S, Béguin F. Nanotubular materials as electrodes for supercapacitors. Fuel Process Technol 2002;77–78:213–9. http://dx.doi.org/10.1016/S0378-3820(02)00078-4 URL ⟨http://linkinghub.elsevier.com/retrieve/pii/S0378382002000784⟩.

[60] Hughes M, Shaffer M, Renouf A, Singh C, Chen G, Fray D, et al. Electrochemical capacitance of nanocomposite films formed by coating aligned arrays of carbon nanotubes with polypyrrole. Adv Mater 2002;14(5):382. http://dx.doi.org/10.1002/1521-4095(20020304)14:5¡382::AID-ADMA382¿3.0.CO;2-Y.

[61] Hughes M, Chen GZ, Shaffer MSP, Fray DJ, Windle AH. Electrochemical capacitance of a nanoporous composite of carbon nanotubes and polypyrrole. Chem Mater 2002;14(4):1610–3. http://dx.doi.org/10.1021/cm010744r URL ⟨http://pubs.acs.org/doi/abs/10.1021/cm010744r⟩.

[62] Arabale G, Wagh D, Kulkarni M, Mulla I, Vernekar S, Vijayamohanan K, et al. Enhanced supercapacitance of multiwalled carbon nanotubes functionalized with ruthenium oxide. Chem Phys Lett 2003;376(1–2):207–13. http://dx.doi.org/10.1016/S0009-2614(03)00946-1 URL ⟨http://linkinghub.elsevier.com/retrieve/pii/S0009261403009461⟩.

[63] Wu Z-S, Zhou G, Yin L-C, Ren W, Li F, Cheng H-M. Graphene/metal oxide composite electrode materials for energy storage. Nano Energy 2012;1 (1):107–31. http://dx.doi.org/10.1016/j.nanoen.2011.11.001 URL ⟨http://linkinghub.elsevier.com/retrieve/pii/S2211285511000176⟩.

[64] Novoselov KS, Geim AK, Morozov SV, Jiang D, Zhang Y, Dubonos SV, et al. Electric field effect in atomically thin carbon films. Science (New York, N.Y.) 2004;306(5696):666–9. http://dx.doi.org/10.1126/science.1102896 URL ⟨http://www.ncbi.nlm.nih.gov/pubmed/15499015⟩.

[65] Novoselov KS, Geim AK, Morozov SV, Jiang D, Katsnelson MI, Grigorieva IV, et al. Two-dimensional gas of massless Dirac fermions in graphene. Nature 2005;438(7065):197–200. http://dx.doi.org/10.1038/nature04233 URL ⟨http://www.ncbi.nlm.nih.gov/pubmed/16281030⟩.

[66] Geim A, Novoselov K. The rise of graphene. Nat Mater 2007:183–91 URL ⟨http://www.nature.com/nmat/journal/v6/n3/abs/nmat1849.html⟩.

[67] Geim A. Graphene: status and prospects. Science (New York, N.Y.) 2009;324 (5934):1530–4. http://dx.doi.org/10.1126/science.1158877 URL ⟨http://www.ncbi.nlm.nih.gov/pubmed/19541989⟩.

[68] Chen H, Müller MB, Gilmore KJ, Wallace GG, Li D. Mechanically strong, electrically conductive, and biocompatible graphene paper. Adv Mater 2008;20(18):3557–61. http://dx.doi.org/10.1002/adma.200800757 URL ⟨http://doi.wiley.com/10.1002/adma.200800757⟩.

[69] Pumera M. Graphene-based nanomaterials and their electrochemistry. Chem Soc Rev 2010;39(11):4146–57. http://dx.doi.org/10.1039/c002690p URL ⟨http://www.ncbi.nlm.nih.gov/pubmed/20623061⟩.

[70] Vivekchand SRC, Rout CS, Subrahmanyam KS, Govindaraj A, Rao CNR. Graphene-based electrochemical supercapacitors. J Chem Sci 2008;120 (1):9–13. http://dx.doi.org/10.1007/s12039-008-0002-7 URL ⟨http://link.springer.com/10.1007/s12039-008-0002-7⟩.

[71] Stoller M, Park S, Zhu Y, An J, Ruoff R. Graphene-based ultracapacitors. Nano Lett 2008:6–10 URL ⟨http://pubs.acs.org/doi/abs/10.1021/nl802558y⟩.

[72] Wang Y, Shi Z, Huang Y, Ma Y. Supercapacitor devices based on graphene materials. J Phys Chem C 2009;113(30):13103–7 URL ⟨http://pubs.acs.org/doi/abs/10.1021/jp902214f⟩.

[73] Xia J, Chen F, Li J, Tao N. Measurement of the quantum capacitance of graphene. Nat Nanotechnol 2009;4(8):505–9. http://dx.doi.org/10.1038/nnano.2009.177 URL ⟨http://www.ncbi.nlm.nih.gov/pubmed/19662012⟩.

[74] Liu C, Yu Z, Neff D, Zhamu A, Jang BZ. Graphene-based supercapacitor with an ultrahigh energy density. Nano Lett 2010:4863–8. http://dx.doi.org/10.1021/nl102661q URL ⟨http://www.ncbi.nlm.nih.gov/pubmed/21058713⟩.

[75] Li N, Tang S, Dai Y, Meng X. The synthesis of graphene oxide nanostructures for supercapacitors: a simple route. J Mater Sci 2014;49(7):2802–9. http://dx.doi.org/10.1007/s10853-013-7986-1 URL ⟨http://link.springer.com/10.1007/s10853-013-7986-1⟩.

[76] Wang D, Li F, Zhao J, Ren W, Chen Z. Fabrication of graphene/polyaniline composite paper via in situ anodic electropolymerization for high-performance flexible electrode. Acs Nano 2009;3(7):1745–52 URL ⟨http://pubs.acs.org/doi/abs/10.1021/nn900297m⟩.

[77] Xu J, Wang K, Zu S, Han B, Wei Z. Hierarchical nanocomposites of polyaniline nanowire arrays on graphene oxide sheets with synergistic effect for energy storage. Acs Nano 2010;4(9):5019–26 URL ⟨http://pubs.acs.org/doi/abs/10.1021/nn1006539⟩.

[78] He Y, Bai D, Yang X, Chen J. A Co (OH) 2 graphene nanosheets composite as a high performance anode material for rechargeable lithium batteries. Electrochem Comm 2010;12(4):570–3. http://dx.doi.org/10.1016/j.elecom.2010.02.002.

[79] Wang H, Casalongue HS, Liang Y, Dai H. Ni(OH)2 nanoplates grown on graphene as advanced electrochemical pseudocapacitor materials. J Am Chem Soc 2010;132(21):7472–7. http://dx.doi.org/10.1021/ja102267j URL ⟨http://www.ncbi.nlm.nih.gov/pubmed/20443559⟩.

[80] Fan Z, Yan J, Zhi L, Zhang Q, Wei T, Feng J, et al. A three-dimensional carbon nanotube/graphene sandwich and its application as electrode in supercapacitors. Adv Mater (Deerfield Beach, Fla.) 2010;22(33):3723–8. http://dx.doi.org/10.1002/adma.201001029 URL ⟨http://www.ncbi.nlm.nih.gov/pubmed/20652901⟩.

[81] Jeong H, Jin M, Ra E, Sheem K. Enhanced electric double layer capacitance of graphite oxide intercalated by poly (sodium 4-styrensulfonate) with high cycle stability. ACS … 2010;4(2):0–4 URL ⟨http://pubs.acs.org/doi/abs/10.1021/nn901790f⟩.

[82] Wang H, Robinson JT, Dianakov G, Dai H. Nanocrystal growth on graphene with various degrees of oxidation. J Am Chem Soc 2010;132(10):3270–1 URL ⟨http://pubs.acs.org/doi/abs/10.1021/ja100329d⟩.

[83] Yan J, Wei T, Shao B, Ma F, Fan Z, Zhang M, et al. Electrochemical properties of graphene nanosheet/carbon black composites as electrodes for supercapacitors. Carbon 2010;48(6):1731–7. http://dx.doi.org/10.1016/j.carbon.2010.01.014 URL ⟨http://linkinghub.elsevier.com/retrieve/pii/S0008622310000370⟩.

[84] Lee JK, Smith KB, Hayner CM, Kung HH. Silicon nanoparticles-graphene paper composites for Li ion battery anodes. Chem Commun (Cambridge, England) 2010;46(12):2025–7. http://dx.doi.org/10.1039/b919738a URL ⟨http://www.ncbi.nlm.nih.gov/pubmed/20221480⟩.

[85] Song Y, Xu J-L, Liu X-X. Electrochemical anchoring of dual doping polypyrrole on graphene sheets partially exfoliated from graphite foil for high-performance supercapacitor electrode. J Power Sources 2014;249:48–58. http://dx.doi.org/10.1016/j.jpowsour.2013.10.102 URL ⟨http://linkinghub.elsevier.com/retrieve/pii/S0378775313017680⟩.

[86] Deng L, Wang J, Zhu G, Kang L, Hao Z, Lei Z, et al. RuO2/graphene hybrid material for high performance electrochemical capacitor. J Power Sources 2014;248:407–15. http://dx.doi.org/10.1016/j.jpowsour.2013.09.081 URL ⟨http://linkinghub.elsevier.com/retrieve/pii/S0378775313015875⟩.

[87] Cai Y, Wang Y, Deng S, Chen G, Li Q, Han B, et al. Graphene nanosheets-tungsten oxides composite for supercapacitor electrode. Ceram Int 2014;40 (3):4109–16. http://dx.doi.org/10.1016/j.ceramint.2013.08.065 URL ⟨http://linkinghub.elsevier.com/retrieve/pii/S0272884213010237⟩.

[88] Wang D, Min Y, Yu Y, Peng B. A general approach for fabrication of nitrogen-doped graphene sheets and its application in supercapacitors. J Colloid Interface Sci 2014;417:270–7. http://dx.doi.org/10.1016/j.jcis.2013.11.021 URL ⟨http://www.ncbi.nlm.nih.gov/pubmed/24407687⟩.

[89] Gopalakrishnan K, Govindaraj A, Rao CNR. Extraordinary supercapacitor performance of heavily nitrogenated graphene oxide obtained by microwave synthesis. J Mater Chem A 2013;1(26):7563. http://dx.doi.org/10.1039/c3ta11385j URL ⟨http://xlink.rsc.org/?DOI=c3ta11385j⟩.

[90] Liang C, Li Z, Dai S. Mesoporous carbon materials: synthesis and modification. Angew Chem (International edition in English) 2008;47(20):3696–717. http://dx.doi.org/10.1002/anie.200702046 URL ⟨http://www.ncbi.nlm.nih.gov/pubmed/18350530⟩.

[91] Saha D, Li Y, Bi Z, Chen J, Keum JK, Hensley DK, et al. Studies on supercapacitor electrode material from activated lignin-derived mesoporous carbon. Langmuir : ACS J Surf Colloids 2014;30(3):900–10. http://dx.doi.org/10.1021/la404112m URL ⟨http://www.ncbi.nlm.nih.gov/pubmed/24400670⟩.

[92] Kumagai S, Sato M, Tashima D. Electrical double-layer capacitance of micro- and mesoporous activated carbon prepared from rice husk and beet sugar. Electrochim Acta 2013;114:617–26. http://dx.doi.org/10.1016/j.electacta.2013.10.060 URL ⟨http://linkinghub.elsevier.com/retrieve/pii/S001346861302015X⟩.

[93] Ahn YR, Song MY, Jo SM, Park CR, Kim DY. Electrochemical capacitors based on electrodeposited ruthenium oxide on nanofibre substrates. Nanotechnology 2006;17(12):2865 URL ⟨http://stacks.iop.org/0957-4484/17/i=12/a=007⟩.

[94] Patake VD, Lokhande CD, Joo OS. Electrodeposited ruthenium oxide thin films for supercapacitor: effect of surface treatments. Appl Surf Sci 2009;255 (7):4192–6. http://dx.doi.org/10.1016/j.apsusc.2008.11.005.

[95] Hu CC, Huang YH, Chang KH. Annealing effects on the physicochemical characteristics of hydrous ruthenium and ruthenium-iridium oxides for electrochemical supercapacitors. J Power Sources 2002;108(1–2):117–27. http://dx.doi.org/10.1016/S0378-7753(02)00011-3.

[96] Yan J, Wei T, Cheng J, Fan Z, Zhang M. Preparation and electrochemical properties of lamellar MnO2 for supercapacitors. Mater Res Bull 2010;45 (2):210–5. http://dx.doi.org/10.1016/j.materresbull.2009.09.016.

[97] Jiang J, Kucernak A. Electrochemical supercapacitor material based on manganese oxide: preparation and characterization. Electrochim Acta 2002;47(15):2381–6. http://dx.doi.org/10.1016/S0013-4686(02)00031-2.

[98] Patil UM, Salunkhe RR, Gurav KV, Lokhande CD. Chemically deposited nanocrystalline NiO thin films for supercapacitor application. Appl Surf Sci 2008;255(5 (Part 2)):2603–7. http://dx.doi.org/10.1016/j.apsusc.2008.07.192.

[99] Nelson PA, Owen JR. A high-performance supercapacitor/battery hybrid incorporating templated mesoporous electrodes. J Electrochem Soc 2003;150(10):A1313. http://dx.doi.org/10.1149/1.1603247 URL ⟨http://jes.ecsdl.org/cgi/doi/10.1149/1.1603247⟩.

[100] Kandalkar SG, Gunjakar JL, Lokhande CD. Preparation of cobalt oxide thin films and its use in supercapacitor application. Appl Surf Sci 2008;254 (17):5540–4. http://dx.doi.org/10.1016/j.apsusc.2008.02.163.

[101] Miura N, Oonishi S, RajendraPrasad K. Indium tin oxide/carbon composite electrode material for electrochemical supercapacitors. Electrochem Solid-State Lett 2004;7(8):A247. http://dx.doi.org/10.1149/1.1763773 URL ⟨http://esl.ecsdl.org/cgi/doi/10.1149/1.1763773⟩.

[102] Hu CC, Huang CM, Chang KH. Anodic deposition of porous vanadium oxide network with high power characteristics for pseudocapacitors. J Power Sources 2008;185(2):1594–7. http://dx.doi.org/10.1016/j.jpowsour.2008.08.017.
[103] da Silva DL, Delatorre RG, Pattanaik G, Zangari G, Figueiredo W, Blum R-P, et al. Electrochemical synthesis of vanadium oxide nanofibers. J Electrochem Soc 2008;155(1):E14. http://dx.doi.org/10.1149/1.2804856 URL ⟨http://jes.ecsdl.org/cgi/doi/10.1149/1.2804856⟩.
[104] Zhou X, Chen H, Shu D, He C, Nan J. Study on the electrochemical behavior of vanadium nitride as a promising supercapacitor material. J Phys Chem Solids 2009;70(2):495–500. http://dx.doi.org/10.1016/j.jpcs.2008.12.004.
[105] Nakayama M, Tanaka A, Sato Y, Tonosaki T, Ogura K. Electrodeposition of manganese and molybdenum mixed oxide thin films and their charge storage properties. Langmuir 2005;21(13):5907–13. http://dx.doi.org/10.1021/la050114u URL ⟨http://pubs.acs.org/doi/abs/10.1021/la050114u⟩.
[106] Babakhani B, Ivey DG. Anodic deposition of manganese oxide electrodes with rod-like structures for application as electrochemical capacitors. J Power Sources 2010;195(7):2110–7. http://dx.doi.org/10.1016/j.jpowsour.2009.10.045.
[107] Lee H, Cho MS, Kim IH, Nam JD, Lee Y. RuOx/polypyrrole nanocomposite electrode for electrochemical capacitors. Synth Metals 2010;160(9–10):1055–9. http://dx.doi.org/10.1016/j.synthmet.2010.02.026 URL ⟨http://linkinghub.elsevier.com/retrieve/pii/S0379677910001037⟩.
[108] Kim I-H, Kim K-B. Electrochemical characterization of hydrous ruthenium oxide thin-film electrodes for electrochemical capacitor applications. J Electrochem Soc 2006;153(2):A383. http://dx.doi.org/10.1149/1.2147406 URL ⟨http://jes.ecsdl.org/cgi/doi/10.1149/1.2147406⟩.
[109] Jia QX, Song SG, Wu XD, Cho JH, Foltyn SR, Findikoglu AT, et al. Epitaxial growth of highly conductive RuO2 thin films on (100) Si. Appl Phys Lett 1996;68(8):1069. http://dx.doi.org/10.1063/1.115715 URL ⟨http://link.aip.org/link/APPLAB/v68/i8/p1069/s1&Agg=doi⟩.
[110] Sakiyama K, Onishi S, Ishihara K. Deposition and properties of reactively sputtered ruthenium dioxide films. J Electrochem Soc 1993;140(3):834–9 URL ⟨http://jes.ecsdl.org/content/140/3/834.short⟩.
[111] Zheng J, Cygan P, Jow T. Hydrous ruthenium oxide as an electrode material for electrochemical capacitors. J Electrochem Soc 1995;142(8):9–13 URL ⟨http://jes.ecsdl.org/content/142/8/2699.short⟩.
[112] Wu N-L, Kuo S-L, Lee M-H. Preparation and optimization of RuO2 -impregnated SnO2 xerogel supercapacitor. J Power Sources 2002;104:62–5.
[113] Hu CC, Lee CH, Wen TC. Oxygen evolution and hypochlorite production on Ru–Pt binary oxides. J Appl Electrochem 1996;26(1):72–82. http://dx.doi.org/10.1007/BF00248191 URL ⟨http://link.springer.com/10.1007/BF00248191⟩.
[114] Ramani M, Haran BS, White RE, Popov BN. Synthesis and characterization of hydrous ruthenium oxide-carbon supercapacitors. J Electrochem Soc 2001;148(4):A374. http://dx.doi.org/10.1149/1.1357172 URL ⟨http://jes.ecsdl.org/cgi/doi/10.1149/1.1357172⟩.
[115] Ferro S, Urgeghe C, Battisti AD. Heterogeneous electron-transfer rate constants for fe(h(2)o)(6)(3+/2+) at metal oxide electrodes. J Phys Chem B 2004;108(20):6398–401. http://dx.doi.org/10.1021/jp049921c URL ⟨http://www.ncbi.nlm.nih.gov/pubmed/18950127⟩.
[116] Wen T, Hu C. Hydrogen and oxygen evolutions on RuIr binary oxides. J Electrochem Soc 1992;139(8):2158–63 URL ⟨http://jes.ecsdl.org/content/139/8/2158.short⟩.
[117] Conway B. Electrochemical supercapacitors: scientific fundamentals and technological applications. New York: Kluwer Academic; 1999.
[118] Zheng J, Jow T. High energy and high power density electrochemical capacitors. J Power Sources 1996;62(2):155–9. http://dx.doi.org/10.1016/S0378-7753(96)02424-X URL ⟨http://linkinghub.elsevier.com/retrieve/pii/S037877539602424X⟩.
[119] Su Y, Wu F, Bao L, Yang Z. RuO 2/activated carbon composites as a positive electrode in an alkaline electrochemical capacitor. New Carbon Mater 2007;22(1):0–4 URL ⟨http://www.sciencedirect.com/science/article/pii/S1872580507600079⟩.
[120] Burke A. Ultracapacitors: why, how, and where is the technology. J Power Sources 2000;91(1):37–50. http://dx.doi.org/10.1016/S0378-7753(00)00485-7 URL ⟨http://linkinghub.elsevier.com/retrieve/pii/S0378775300004857⟩.
[121] Yu G-Y, Chen W-X, Zheng Y-F, Zhao J, Li X, Xu Z-D. Synthesis of Ru/carbon nanocomposites by polyol process for electrochemical supercapacitor electrodes. Mater Lett 2006;60(20):2453–6. http://dx.doi.org/10.1016/j.matlet.2006.01.015 URL ⟨http://linkinghub.elsevier.com/retrieve/pii/S0167577X06000577⟩.
[122] Seo M-K, Saouab A, Park S-J. Effect of annealing temperature on electrochemical characteristics of ruthenium oxide/multi-walled carbon nanotube composites. Mater Sci Eng: B 2010;167(1):65–9. http://dx.doi.org/10.1016/j.mseb.2010.01.028 URL ⟨http://linkinghub.elsevier.com/retrieve/pii/S0921510710000486⟩.
[123] Zheng Y-Z, Ding H-Y, Zhang M-L. Hydrousrutheniumoxide thin film electrodes prepared by cathodic electrodeposition for supercapacitors. Thin Solid Films 2008;516(21):7381–5. http://dx.doi.org/10.1016/j.tsf.2008.02.022 URL ⟨http://linkinghub.elsevier.com/retrieve/pii/S0040609008002344⟩.
[124] Kim Y-T, Tadai K, Mitani T. Highly dispersed ruthenium oxide nanoparticles on carboxylated carbon nanotubes for supercapacitor electrode materials. J Mater Chem 2005;15(46):4914. http://dx.doi.org/10.1039/b511869g URL ⟨http://xlink.rsc.org/?DOI=b511869g⟩.
[125] Lee J-K, Pathan HM, Jung K-D, Joo O-S. Electrochemical capacitance of nanocomposite films formed by loading carbon nanotubes with ruthenium oxide. J Power Sources 2006;159(2):1527–31. http://dx.doi.org/10.1016/j.jpowsour.2005.11.063 URL ⟨http://linkinghub.elsevier.com/retrieve/pii/S0378775305016319⟩.
[126] Hu C-C, Chen W-C, Chang K-H. How to achieve maximum utilization of hydrous ruthenium oxide for supercapacitors. J Electrochem Soc 2004;151(2):A281. http://dx.doi.org/10.1149/1.1639020 URL ⟨http://jes.ecsdl.org/cgi/doi/10.1149/1.1639020⟩.
[127] Long J, Swider K, Merzbacher C, Rolison D. Voltammetric characterization of ruthenium oxide-based aerogels and other RuO2 solids: the nature of capacitance in nanostructured materials. Langmuir 1999;15(3):780–5 URL ⟨http://pubs.acs.org/doi/abs/10.1021/la980785a⟩.
[128] Sugimoto W, Iwata H, Yokoshima K, Murakami Y, Takasu Y. Proton and electron conductivity in hydrous ruthenium oxides evaluated by electrochemical impedance spectroscopy: the origin of large capacitance. J Phys Chem B 2005;109(15):7330–8. http://dx.doi.org/10.1021/jp044252o URL ⟨http://www.ncbi.nlm.nih.gov/pubmed/16851839⟩.
[129] Zheng J, Jow T. A new charge storage mechanism for electrochemical capacitors. J Electrochem Soc 1995;142(1):14–6 URL ⟨http://jes.ecsdl.org/content/142/1/L6.short⟩.
[130] McKeown D, Hagans P, Carette LPL, Russell AE, Swider KE, Rolison DR. Structure of hydrous ruthenium oxides: implications for charge storage. J Phys Chem B 1999;103(23):4825–32 URL ⟨http://pubs.acs.org/doi/abs/10.1021/jp990096n⟩.
[131] Hu C-C, Chang K-H, Lin M-C, Wu Y-T. Design and tailoring of the nanotubular arrayed architecture of hydrous RuO2 for next generation supercapacitors. Nano Lett 2006;6(12):2690–5. http://dx.doi.org/10.1021/nl061576a URL ⟨http://www.ncbi.nlm.nih.gov/pubmed/17163689⟩.
[132] Sugimoto W, Yokoshima K, Murakami Y, Takasu Y. Charge storage mechanism of nanostructured anhydrous and hydrous ruthenium-based oxides. Electrochim Acta 2006;52(4):1742–8. http://dx.doi.org/10.1016/j.electacta.2006.02.054 URL ⟨http://linkinghub.elsevier.com/retrieve/pii/S0013468606004178⟩.
[133] Wen J, Ruan X, Zhou Z. Preparation and electrochemical performance of novel ruthenium-manganese oxide electrode materials for electrochemical capacitors. J Phys Chem Solids 2009;70(5):816–20. http://dx.doi.org/10.1016/j.jpcs.2009.03.015 URL ⟨http://dx.doi.org/10.1016/j.jpcs.2009.03.015⟩.
[134] Foelske A, Barbieri O, Hahn M, Kotz R. An X-ray photoelectron spectroscopy study of hydrous ruthenium oxide powders with various water contents for supercapacitors. Electrochem Solid-State Lett 2006;9(6):A268. http://dx.doi.org/10.1149/1.2188078 URL ⟨http://esl.ecsdl.org/cgi/doi/10.1149/1.2188078⟩.
[135] Kim H, Popov BN. Characterization of hydrous ruthenium oxide/carbon nanocomposite supercapacitors prepared by a colloidal method. J Power Sources 2002;104(1):52–61. http://dx.doi.org/10.1016/S0378-7753(01)00903-X URL ⟨http://linkinghub.elsevier.com/retrieve/pii/S037877530100903X⟩.
[136] Subramanian V. Mesoporous anhydrous RuO2 as a supercapacitor electrode material. Solid State Ionics 2004;175(1-4):511–5. http://dx.doi.org/10.1016/j.ssi.2004.01.070 URL ⟨http://linkinghub.elsevier.com/retrieve/pii/S0167-2738(04)00627-7⟩.
[137] Egashira M, Matsuno Y, Yoshimoto N, Morita M. Pseudo-capacitance of composite electrode of ruthenium oxide with porous carbon in non-aqueous electrolyte containing imidazolium salt. J Power Sources 2010;195(9):3036–40. http://dx.doi.org/10.1016/j.jpowsour.2009.11.046 URL ⟨http://linkinghub.elsevier.com/retrieve/pii/S0378775309020540⟩.
[138] Lin YS, Lee KY, Chen KY, Huang YS. Superior capacitive characteristics of RuO2 nanorods grown on carbon nanotubes. Appl Surf Sci 2009;256(4):1042–5. http://dx.doi.org/10.1016/j.apsusc.2009.08.026.
[139] Takasu Y, Nakamura T. Dip coated RuV oxide electrodes for electrochemical capacitors. J Electrochem Soc 1997;144(8):2601–6 URL ⟨http://jes.ecsdl.org/content/144/8/2601.short⟩.
[140] Yuan C-Z, Gao B, Zhang X-G. Electrochemical capacitance of NiO/Ru0.35V0.65O2 asymmetric electrochemical capacitor. J Power Sources 2007;173(1):606–12. http://dx.doi.org/10.1016/j.jpowsour.2007.04.034 URL ⟨http://linkinghub.elsevier.com/retrieve/pii/S0378775307008105⟩.
[141] Yong-gang W, Xiao-gang Z. Preparation and electrochemical capacitance of RuO2/TiO2 nanotubes composites. Electrochim Acta 2004;49(12):1957–62. http://dx.doi.org/10.1016/j.electacta.2003.12.023 URL ⟨http://linkinghub.elsevier.com/retrieve/pii/S0013468603010430⟩.
[142] Pang S-C, Anderson Ma, Chapman TW. novel electrode materials for thin-film ultracapacitors: comparison of electrochemical properties of sol–gel-derived and electrodeposited manganese dioxide. J Electrochem Soc 2000;147(2):444. http://dx.doi.org/10.1149/1.1393216 URL ⟨http://jes.ecsdl.org/cgi/doi/10.1149/1.1393216⟩.
[143] Toupin M, Brousse T, Bélanger D. Influence of microstructure on the charge storage properties of chemically synthesized manganese dioxide. Chem Mater 2002;14(9):3946–52 URL ⟨http://pubs.acs.org/doi/abs/10.1021/cm020408q⟩.
[144] Toupin M, Brousse T, Belanger D. Charge storage mechanism of MnO2 electrode used in aqueous electrochemical capacitor. Chem Mater 2004;16(16):3184–90 URL ⟨http://pubs.acs.org/doi/abs/10.1021/cm049649j⟩.
[145] Chang J-K, Lee M-T, Tsai W-T. In situ Mn K-edge X-ray absorption spectroscopic studies of anodically deposited manganese oxide with relevance to supercapacitor applications. J Power Sources 2007;166(2):590–4. http://dx.doi.org/10.1016/j.jpowsour.2007.01.036 URL ⟨http://linkinghub.elsevier.com/retrieve/pii/S0378775307001954⟩.
[146] Hu C-C, Tsou T-W. Ideal capacitive behavior of hydrous manganese oxide prepared by anodic deposition. Electrochem Commun 2002;4:105–9 URL ⟨http://www.sciencedirect.com/science/article/pii/S1388248101002855⟩.

[147] Messaoudi B, Joiret S, Keddam M, Takenouti H. Anodic behaviour of manganese in alkaline medium. Electrochim Acta 2001;46(16):2487–98. http://dx.doi.org/10.1016/S0013-4686(01)00449-2 URL ⟨http://linkinghub.elsevier.com/retrieve/pii/S0013468601004492⟩.
[148] Raymundo-Pinero E, Khomenko V, Frackowiak E, Beguin F. Performance of manganese oxide/CNTs composites as electrode materials for electrochemical capacitors. J Electrochem Soc 2005;152(1):A229. http://dx.doi.org/10.1149/1.1834913 URL ⟨http://jes.ecsdl.org/cgi/doi/10.1149/1.1834913⟩.
[149] Ye C, Lin ZM, Hui SZ. Electrochemical and capacitance properties of rod-shaped MnO[sub 2] for supercapacitor. J Electrochem Soc 2005;152(6):A1272. http://dx.doi.org/10.1149/1.1904912 URL ⟨http://jes.ecsdl.org/cgi/doi/10.1149/1.1904912⟩.
[150] Kim H, Popov BN. Synthesis and characterization of MnO[sub 2]-based mixed oxides as supercapacitors. J Electrochem Soc 2003;150(3):D56. http://dx.doi.org/10.1149/1.1541675 URL ⟨http://jes.ecsdl.org/cgi/doi/10.1149/1.1541675⟩.
[151] Lee M-T, Chang J-K, Tsai W-T. Effects of iron addition on material characteristics and pseudo-capacitive behavior of Mn-oxide electrodes. J Electrochem Soc 2007;154(9):A875. http://dx.doi.org/10.1149/1.2755880 URL ⟨http://jes.ecsdl.org/cgi/doi/10.1149/1.2755880⟩.
[152] Chang J-K, Huang C-H, Lee M-T, Tsai W-T, Deng M-J, Sun I-W. Physicochemical factors that affect the pseudocapacitance and cyclic stability of Mn oxide electrodes. Electrochim Acta 2009;54(12):3278–84. http://dx.doi.org/10.1016/j.electacta.2008.12.042 URL ⟨http://linkinghub.elsevier.com/retrieve/pii/S0013468608014412⟩.
[153] Wei J, Nagarajan N, Zhitomirsky I. Manganese oxide films for electrochemical supercapacitors. J Mater Process Technol 2007;186(1-3):356–61. http://dx.doi.org/10.1016/j.jmatprotec.2007.01.003 URL ⟨http://linkinghub.elsevier.com/retrieve/pii/S0924013607000179⟩.
[154] Donne S, Hollenkamp AF, Jones B. Structure, morphology and electrochemical behaviour of manganese oxides prepared by controlled decomposition of permanganate. J Power Sources 2010;195(1):367–73. http://dx.doi.org/10.1016/j.jpowsour.2009.06.103 URL ⟨http://linkinghub.elsevier.com/retrieve/pii/S0378775309011781⟩.
[155] Chou S, Cheng F, Chen J. Electrodeposition synthesis and electrochemical properties of nanostructured γ-MnO2 films. J Power Sources 2006;162(1):727–34. http://dx.doi.org/10.1016/j.jpowsour.2006.06.033 URL ⟨http://linkinghub.elsevier.com/retrieve/pii/S0378775306011888⟩.
[156] Brousse T, Toupin M, Dugas R, Athouel L, Crosnier O, Belanger D. Crystalline MnO[sub 2] as possible alternatives to amorphous compounds in electrochemical supercapacitors. J Electrochem Soc 2006;153(12):A2171. http://dx.doi.org/10.1149/1.2352197 URL ⟨http://jes.ecsdl.org/cgi/doi/10.1149/1.2352197⟩.
[157] Zolfaghari A, Ataherian F, Ghaemi M, Gholami A. Capacitive behavior of nanostructured MnO2 prepared by sonochemistry method. Electrochim Acta 2007;52(8):2806–14. http://dx.doi.org/10.1016/j.electacta.2006.10.035 URL ⟨http://linkinghub.elsevier.com/retrieve/pii/S0013468606010930⟩.
[158] Ghaemi M, Ataherian F, Zolfaghari A, Jafari S. Charge storage mechanism of sonochemically prepared MnO2 as supercapacitor electrode: effects of physisorbed water and proton conduction. Electrochim Acta 2008;53(14):4607–14. http://dx.doi.org/10.1016/j.electacta.2007.12.040 URL ⟨http://linkinghub.elsevier.com/retrieve/pii/S0013468607015009⟩.
[159] Nagarajan N, Cheong M, Zhitomirsky I. Electrochemical capacitance of MnOx films. Mater Chem Phys 2007;103(1):47–53. http://dx.doi.org/10.1016/j.matchemphys.2007.01.005 URL ⟨http://linkinghub.elsevier.com/retrieve/pii/S0254058407000089⟩.
[160] Hu C-C, Wang C-C. Nanostructures and capacitive characteristics of hydrous manganese oxide prepared by electrochemical deposition. J Electrochem Soc 2003;150(8):A1079. http://dx.doi.org/10.1149/1.1587725 URL ⟨http://jes.ecsdl.org/cgi/doi/10.1149/1.1587725⟩.
[161] Nagarajan N, Humadi H, Zhitomirsky I. Cathodic electrodeposition of MnOx films for electrochemical supercapacitors. Electrochim Acta 2006;51(15):3039–45. http://dx.doi.org/10.1016/j.electacta.2005.08.042 URL ⟨http://linkinghub.elsevier.com/retrieve/pii/S0013468605010303⟩.
[162] Chang J-K, Huang C-H, Tsai W-T, Deng M-J, Sun I-W, Chen P-Y. Manganese films electrodeposited at different potentials and temperatures in ionic liquid and their application as electrode materials for supercapacitors. Electrochim Acta 2008;53(13):4447–53. http://dx.doi.org/10.1016/j.electacta.2008.01.036 URL ⟨http://linkinghub.elsevier.com/retrieve/pii/S0013468608000856⟩.
[163] Liu F-J. Electrodeposition of manganese dioxide in three-dimensional poly(3,4-ethylenedioxythiophene)poly(styrene sulfonic acid) polyaniline for supercapacitor. J Power Sources 2008;182(1):383–8. http://dx.doi.org/10.1016/j.jpowsour.2008.04.008 URL ⟨http://linkinghub.elsevier.com/retrieve/pii/S0378775308006472⟩.
[164] Nam K-W, Lee C-W, Yang X-Q, Cho BW, Yoon W-S, Kim K-B. Electrodeposited manganese oxides on three-dimensional carbon nanotube substrate: supercapacitive behaviour in aqueous and organic electrolytes. J Power Sources 2009;188(1):323–31. http://dx.doi.org/10.1016/j.jpowsour.2008.11.133 URL ⟨http://linkinghub.elsevier.com/retrieve/pii/S0378775308022805⟩.
[165] Chin S-F, Pang S-C, Anderson Ma. Material and electrochemical characterization of tetrapropylammonium manganese oxide thin films as novel electrode materials for electrochemical capacitors. J Electrochem Soc 2002;149(4):A379. http://dx.doi.org/10.1149/1.1453406 URL ⟨http://jes.ecsdl.org/cgi/doi/10.1149/1.1453406⟩.
[166] Shinomiya T, Gupta V, Miura N. Effects of electrochemical-deposition method and microstructure on the capacitive characteristics of nano-sized manganese oxide. Electrochim Acta 2006;51(21):4412–9. http://dx.doi.org/10.1016/j.electacta.2005.12.025 URL ⟨http://linkinghub.elsevier.com/retrieve/pii/S0013468605014003⟩.
[167] Broughton J, Brett M. Investigation of thin sputtered Mn films for electrochemical capacitors. Electrochim Acta 2004;49(25):4439–46. http://dx.doi.org/10.1016/j.electacta.2004.04.035 URL ⟨http://linkinghub.elsevier.com/retrieve/pii/S0013468604004591⟩.
[168] Rajendra Prasad K, Miura N. Electrochemically synthesized MnO2-based mixed oxides for high performance redox supercapacitors. Electrochem Commun 2004;6(10):1004–8. http://dx.doi.org/10.1016/j.elecom.2004.07.017 URL ⟨http://linkinghub.elsevier.com/retrieve/pii/S1388248104002061⟩.
[169] Reddy RN, Reddy RG. Synthesis and electrochemical characterization of amorphous MnO2 electrochemical capacitor electrode material. J Power Sources 2004;132(1–2):315–20. http://dx.doi.org/10.1016/j.jpowsour.2003.12.054 URL ⟨http://linkinghub.elsevier.com/retrieve/pii/S0378775304000709⟩.
[170] Levine K. Synthesis, characterization and properties of polypyrrole/polyimide composites [Ph.D. thesis]. University of Cincinnati; 2002.
[171] Arbizzani C, Mastragostino M, Meneghello L. Polymer-based redox supercapacitors: a comparative study. Electrochim Acta 1996;41(1):21–6. http://dx.doi.org/10.1016/0013-4686(95)00289-Q URL ⟨http://linkinghub.elsevier.com/retrieve/pii/001346869500289Q⟩.
[172] Mastragostino M, Arbizzani C, Soavi F. Polymer-based supercapacitors. J Power Sources 2001;97-98:812–5. http://dx.doi.org/10.1016/S0378-7753(01)00613-9 URL ⟨http://linkinghub.elsevier.com/retrieve/pii/S0378775301006139http://www.sciencedirect.com/science/article/pii/S0378775301006139⟩.
[173] Arbizzani C, Mastragostino M, Soavi F. New trends in electrochemical supercapacitors. J Power Sources 2001;100:164–70 URL ⟨http://www.sciencedirect.com/science/article/pii/S0378775301008928⟩.
[174] Frackowiak E, Khomenko V, Jurewicz K, Lota K, Béguin F. Supercapacitors based on conducting polymers/nanotubes composites. J Power Sources 2006;153(2):413–8. http://dx.doi.org/10.1016/j.jpowsour.2005.05.030 URL ⟨http://linkinghub.elsevier.com/retrieve/pii/S0378775305007391⟩.
[175] Haushalter RC, Krause LJ. Electron-less metallization of organic polymers using the polymer as a redox reagent: reaction of polyimide with zintl anions. Thin Solid Films 1983;102:161–71. http://dx.doi.org/10.1016/0040-6090(83)90149-9 URL ⟨⟩.
[176] Pell WG, Conway BE. Voltammetry at a de Levie brush electrode as a model for electrochemical supercapacitor behaviour. J Electroanal Chem 2001;500(1–2):121–33. http://dx.doi.org/10.1016/S0022-0728(00)00423-X.
[177] Halper M, Ellenbogen J. Supercapacitors: a brief overview. Technical report March, MITRE Nanosystems Group; 2006. URL ⟨http://www.srv1.mitre.org/work/tech_papers/tech_papers_06/06_0667/06_0667.pdfhttp://www.mitre.org/sites/default/files/pdf/06_0667.pdf⟩.
[178] Galiński M, Lewandowski A, Stępniak I. Ionic liquids as electrolytes. Electrochim Acta 2006;51(26):5567–80. http://dx.doi.org/10.1016/j.electacta.2006.03.016 URL ⟨http://linkinghub.elsevier.com/retrieve/pii/S0013468606002362⟩.
[179] Liu H, Liu Y, Li J. Ionic liquids in surface electrochemistry. Phys Chem Chem Phys: PCCP 2010;12(8):1648. http://dx.doi.org/10.1039/b921469k URL ⟨http://www.ncbi.nlm.nih.gov/pubmed/20145828⟩.
[180] Armand M, Endres F, MacFarlane DR, Ohno H, Scrosati B. Ionic-liquid materials for the electrochemical challenges of the future. Nat Mater 2009;8(8):621–9. http://dx.doi.org/10.1038/nmat2448 URL ⟨http://www.ncbi.nlm.nih.gov/pubmed/19629083⟩.
[181] Cericola D, Kötz R. Hybridization of rechargeable batteries and electrochemical capacitors: principles and limits. Electrochim Acta 2012;72:1–17. http://dx.doi.org/10.1016/j.electacta.2012.03.151 URL ⟨http://dx.doi.org/10.1016/j.electacta.2012.03.151⟩.
[182] Miller JM. Ultracapacitor applications, IET; 2011.
[183] Belyakov AI. Asymmetric electrochemical supercapacitors with aqueous electrolytes. In: ESSCAP'08, vol. 3, Roma; 2008.
[184] Sivakkumar S, Pandolfo AG. Evaluation of lithium-ion capacitors assembled with pre-lithiated graphite anode and activated carbon cathode. Electrochim Acta 2012;65:280–7. http://dx.doi.org/10.1016/j.electacta.2012.01.076 URL ⟨http://linkinghub.elsevier.com/retrieve/pii/S0013468612001144⟩.
[185] Christen T, Carlen MW. Theory of Ragone plots. J Power Sources 2000;91(2):210–6. http://dx.doi.org/10.1016/S0378-7753(00)00474-2.
[186] Díaz M, Ortiz A, Ortiz I. Progress in the use of ionic liquids as electrolyte membranes in fuel cells. J Membr Sci 2014;469:379–96. http://dx.doi.org/10.1016/j.memsci.2014.06.033 URL ⟨http://dx.doi.org/10.1016/j.memsci.2014.06.033⟩.
[187] Chen K, Xue D. Water-soluble inorganic salt with ultrahigh specific capacitance: Ce(NO3)3 can be designed as excellent pseudocapacitor electrode. J Colloid Interface Sci 2014;416(3):172–6. http://dx.doi.org/10.1016/j.jcis.2013.10.044.